QUANTIFICATION OF ORGANIC CARBON IN BIOCHAR AMENDED SOIL USING GROUND PENETRATING RADAR (GPR)

A Thesis

by

XIAOQING SHEN

Submitted to the Office of Graduate and Professional Studies of
Texas A&M University
in partial fulfillment of the requirements for the degree of

MASTER OF SCIENCE

Chair of Committee,	Russell Jessup
Committee Members,	Dirk Hays
	Byron Burson
	Rodante Tabien
Head of Department,	David Baltensperger

August 2019

Major Subject: Plant Breeding

ABSTRACT

The application of biochar soil amendments has been proposed as a strategy of mitigating global carbon emissions and soil organic carbon loss. Biochar can provide additional agronomic benefits to cropping systems, including improved crop yield, soil water holding capacity, seed germination, cation exchange capacity (CEC), and soil pH. Commercial development of biochar amendments has been limited; however, their significant potential impacts emphasize the need for further research. In order to maximize beneficial effects of biochar amendments towards the inventory, increase, and management of soil organic carbon (SOC) pools, non-destructive methods to identify and quantify belowground carbon are necessary. Ground penetrating radar (GPR) is potentially one such tool. GPR has been well characterized across geology, archeology, engineering, and military applications. While it has been predominantly utilized to detect relatively large objects such as rocks, tree roots, groundwater, ice, and peat soils, the purpose of this study is to quantify comparatively smaller, particulate sources of soil organic carbon. This research uses three different materials as different carbon source, biochar, graphite, and activated carbon. Mixing with sand, there are twelve treatments in total. GPR attribute analyses, including Pearson correlation, Spearman rank correlation, and naïve Bayes predictive models, were utilized in lieu of visualization methods due to

the minute sized carbon particles of interest. Significant correlation coefficients between attributes and carbon content were found, and the correlation between attributes and moisture level was also significant. The predictive model was able to identify differences in both carbon content and carbon structure.

DEDICATION

This thesis is dedicated to my parents, Ping Jiang and Jin Shen, who encouraged and financially supported me to study abroad. I couldn't accomplish the work I have done without them funding most of my tuition and fees, as well as the constant phone calls whenever I need them. I'd also like to thank all the friends I have made along the way. Overcoming 12 hours of time gap, we can share our lives and feeling regardless the distance.

ACKNOWLEDGEMENTS

I would like to thank my committee chair, Dr. Jessup, and my committee members, Dr. Hays, Dr. Burson, and Dr. Tabien for their guidance and support throughout the course of this research.

Thanks also go to my friends and colleagues and the department faculty and staff for making my time at Texas A&M University a great experience.

CONTRIBUTORS AND FUNDING SOURCES

Contributors

This work was supervised by a thesis committee consisting of Associate Professor and Chair Dr. Russell Jessup. Research Geneticist and Committee Member Dr. Byron Burson of USDA-ARS, Associate Professor and Committee Member Dr. Rodante Tabien of the Soil and Crop Science Department, and Professor and Committee Member Dr. Dirk Hays of Molecular and Environmental Plant Science for allowing me to collect data with the radar prototype.

I would like to recognize research associate Iliyana Dobreva for her guidance and insights regarding computer programming, and providing help towards wavelet analysis, I would also like to thank research associate Henry Ruiz for providing data pre-processing functions and assistance with programming technical issues. I would also like to thank graduate student Matthew Wolfe for assistance in collecting the data with me during the summer.

All other work conducted for the thesis was completed by Xiaoqing Shen independently.

Funding Sources

Graduate study tuition and fee was mostly self-fund, part of the tuition was founded by Dr. Russell Jessup.

This research and the position as Student Technician was supported by United States Department of Energy.

NOMENCLATURE

SOC	Soil Organic Carbon
GPR	Ground Penetrating Radar
ANOVA	Analysis of Variance
ROC	Receiver Operating Characteristic
AUC	Area Under Curve

TABLE OF CONTENTS

Page

LIST OF FIGURES

Page

LIST OF TABLES

Page

CHAPTER I

INTRODUCTION

It has been decades since climate change became of great concern and started debates (Plass, 1956). Climate change can be described as a phenomenon with significant potential impacts on global temperature, polar regions, forests, and freshwater resources. It similarly disturbs agriculture, including crop productivity, soil health, and water resources (Howden et al., 2007, Piao et al., 2010). The resulting risk of decreasing crop production further drives the need for increased land use and soil fertilization; however, this often occurs at the sacrifice of the soil's organic carbon (SOC). This cycle consequently leads to significant SOC loss. With the ability of SOC carbon sequestration and greenhouse gas reduction, loss of SOC eventually leads to less mitigating climate change potential (Batjes,1998; Schimel et al., 2001; Lehmann et al., 2006; Singh et al., 2010). This research addresses the importance of SOC and investigate novel methods to detect and quantify the organic carbon in a non-destructive way. Biochar will be utilized to simulate SOC. Biochar has potential to increase soil organic carbon stocks as a soil amendment (Sombroek, 1993; Glaser et al., 2001; Lehmann et al., 2006; Fowles, 2007; Lehmann, 2007; Laird, 2008; Woolf et al., 2010). Upon detecting and quantifying biochar, results from this study can be extended to further research on soil carbon directly. Traditionally, soil carbon has been quantified by randomly taking core samples from the field to the lab and then analyzing their composition. One of the main goals of the proposed research is to quantify soil carbon without disturbing the soil. Novel, non-

destructive approaches such as ground penetrating radar (GPR) could provide such a tool. Inspired by the study of seismology, GPR can be referred to as radio echo sound that projects pulses of electromagnetic signals into the ground and then receives and records the signals sent back (Jol, 2007). By analyzing many different characteristics of the signal, GPR has been widely applied to explore belowground structures and features involving different fields of study. The most common application is to detect belowground objects such as rocks, buried ancient sites, roots, and underground storage tanks (Butnor et al., 2001; Gader et al., 2001; Stokes et al., 2002; Nicolotti et al., 2003; Cassidy and Jol, 2008; Le Gall et al., 2008; Ng et al., 2008, Dogan et al., 2016). Compared to these applications, fewer studies have investigated smaller subjects such as soil organic matter. Therefore, this research explores the possibility of applying GPR on quantifying carbon in biochar amended soil with activated carbon and graphite as comparative checks possessing structural differences. The model developed will have potential for mapping global soil organic carbon.

CHAPTER II

LITERATURE REVIEW

Significant Role of Carbon

Severe Soil Organic Carbon Pool Loss

The transition of global land resources into managed agricultural systems has greatly changed the terrestrial carbon balance, and this phenomenon has been accelerated in recent decades because of the increase in human population and the increase demand for food, feed, fiber, and fuel (Schimel et al., 2001; Amundson et al., 2015; Montanarella et al., 2016). Land use changes into cropland and grassland systems have resulted in a significant loss of SOC, which is the dominant component of soil organic matter (SOM). Prior to the Industrial Revolution (ca. 1750), global CO_2 emissions were estimated to be 0.011 Gt (Gt = 1 x 10^{12} kg = 1trillion kilograms) per year (Boden et al., 2011). With the rapid increase of industrial scale fossil-fuel utilization, annual CO_2 emissions increased to 0.20 Gt by 1850 and to 1.96 Gt by 1900 (Li, 2000; Boden et al., 2011). The CO_2 emission rate has continued to increase, reaching 24.75 Gt in 2000 and 34.84 Gt in 2011(Herzog, 2001; Boden et al., 2011). An estimated 30 to 60 Pg (Pg = 1 x 10^{12} kg = 1 trillion metric tons) of SOC has been lost over the past 100 years (Scharpenseel and Becker-Heidmann, 1994; Lal, 2001), and cumulative historic SOC losses of about 230 Pg have been reported (Lal, 2001; Lal, 2011). It has been proposed that the reversal of this trend and the future increase of soil carbon stocks can significantly benefit terrestrial ecosystems through carbon sequestration and greenhouse

gas reduction (Batjes,1998; Schimel et al., 2001; Lehmann et al., 2006; Singh et al., 2010).

Strategies to Increase Soil Organic Carbon

Due to the importance of SOC in the carbon cycle and its specific capacity for CO_2 sequestration, novel strategies for increasing the soil organic carbon pool are critical (Post and Kwon, 2000; West and Post, 2002; Schlesinger, 2005; De Deyn et al., 2008; Crowther et al., 2016). Incorporation of stable, recalcitrant carbon into soils via biochar amendments is one potential approach. In one example, 10 t ha^{-1} and 40 t ha^{-1} biochar amendments applied to rice demonstrated no significant difference in carbon intensity of rice production (GHGI) and global warming potential (GWP). Both overall GWP and GHGI decreased from 18.7% to 7.1% and 34.8% to 12.4%, respectively, indicating the potential of biochar amendment for reducing global warming (Zhang et al., 2012). In addition, being highly recalcitrant to decomposition, biochar can significantly slow the rate at which photosynthetically fixed carbon (C) is returned to the atmosphere (Sombroek, 1993; Glaser et al., 2001; Lehmann et al., 2006; Fowles, 2007; Lehmann, 2007; Laird, 2008; Woolf et al., 2010). Biochar can further offset other greenhouse gases including nitrous oxide and methane (Rondon et al., 2005; Clough et al., 2010; van Zwieten et al., 2010; Shackley, 2011). Biochar amendments also have been shown to improve plant growth, increase soil water holding capacity, increase nutrient retention and availability, and reduce pesticide run-off (Gaunt and Lehmann, 2008; Lenton et al., 2009; Shackley, 2011; Yu et al., 2017).

Biochar Production

Pyrolysis, the thermal decomposition of organic materials at elevated temperatures in the absence of oxygen, produces biochar and other byproducts (Shackley, 2011). This process can be divided into two major types, fast pyrolysis and slow pyrolysis. However, these two categories have no precise definitions and are somewhat arbitrary (Mohan et al., 2006; Woolf et al., 2010). Slow pyrolysis is applied at low to moderate temperatures around 300°C and includes relatively long reaction periods up to several days (Onay and Kockar, 2003). The two products produced under these conditions are biochar and pyrolysis gas, which includes high yields of char (as much as 40 wt-%) but also a relatively low-value pyrolysis gas. In contrast, fast pyrolysis involves higher temperatures of approximately 500°C or higher and incubation times as short as 1 to 5 seconds (Bridgwater et al., 1999). Fast pyrolysis can maximize the production of bio-oil with biochar and result in higher energy value products, but the process also has a higher energy investment cost (Brown and Brown, 2013). Biochar, made by slow and fast pyrolysis, have different physicochemical qualities which provide differentiated effects upon the soil environment when applied (Bruun et al., 2012).

Non-destructive Soil Carbon Assessment

To maximize the beneficial effects of biochar amendment applications towards global SOC pools, a rapid, non-destructive and inexpensive method to detect and quantify belowground carbon is needed. GPR has been proposed as such a tool. In contrast, conventional means to detect and quantify soil carbon involve coring, probing, and diverse chemical determination assays. During the process of collecting and

handling samples, oxidation, volatilization, microbial degradation, and other sampling biases often occur (Schumacher, 2002; Hammes et al., 2007; McClellan et al., 2017). Previous applications of GPR across diverse scientific fields have focused on relatively large-scale objects such as ancient cites, land mines, rocks, tree roots, ice, and groundwater (Butnor et al., 2001; Gader et al., 2001; Stokes et al., 2002; Nicolotti et al., 2003; Cassidy and Jol, 2008; Le Gall et al., 2008; Ng et al., 2008, Dogan et al., 2016).

Former GPR Application

It has been proposed that soil organic carbon density can be estimated using GPR (Li et al., 2015). Depending on the objectives of previous studies, GPR has been utilized with varied operating conditions. For instance, as the size of the targeted subject-matter decreases, the frequency of GPR required for detection has tended to increase (Benedetto and Tosti, 2013; Feng et al., 2015; Li et al., 2015; McClellan et al., 2017). Other research has further shown that water impacts dielectric properties and increasing water content results in decreasing radar velocity and increasing attenuation (Topp et al., 1980; Olhoeft, 1987; Li et al., 2015). Despite these challenges, researchers have successfully used GPR to estimate carbon stocks in wetlands (McClellan et al., 2017). Peat soils also have been evaluated with GPR for morphology, volume, and thickness (Parsekian et al., 2012; Loisel et al., 2013). These examples provide a rationale and framework to develop novel GPR methods for biochar and SOC quantification across major soil types worldwide (Jol and Smith, 1995; Iryanti, 2013; Comas et al., 2015).

Promising Strategies Considering Material Identification

Much of the previous GPR research has focused on material identification spanning civil engineering and archaeology (El-Mahallawy and Hashim, 2013; Solla, 2014; Anbazhagan et al., 2016). Relying on time and frequency domain of the signals, wavelet transformation can visualize signal changes and further identify materials. Since in this study, only silicon sand and different carbon sources would be the materials, some methodologies have the potential to analyze the GPR data collected. However, the soil organic carbon particle size is vastly smaller than typical experimental objects targeted in civil engineering and archaeological studies. Visualization of such minute objects is debatable; therefore, a quantification tool is needed (Butnor et al., 2001; Gader et al., 2001; Stokes et al., 2002; Nicolotti et al., 2003; Cassidy and Jol, 2008; Le Gall et al., 2008; Ng et al., 2008, Dogan et al., 2016). Wavelet analysis and attribute analysis were selected to analyze collected data, and a naïve Bayes predictive model was applied to train collected data.

Wavelet Analysis

Wavelet analysis is based on signal data collected by a variety of sensors, and for GPR, it is effective at filtering noise and analyzing signals (Lee and Yamamoto, 1994; Zhu et al, 2009; Javadi and Ghasemzadeh, 2017). With wavelet transformation of signals, their time and frequency domain change corresponding to the scale chosen. With control of the scales, different scales of wavelets will pass through the data collected while generating a coefficient (Lee and Yamamoto, 1994). There are two types of wavelet transforms, continuous wavelet transforms and discrete wavelet transform.

Continuous wavelet transform allows the translating and scale parameter of wavelets to vary continuously, and discrete wavelet transform allows wavelets vary discretely (Heil, 1989). Application of wavelet analysis on GPR data and plotting time-frequency domain can visualize the signal change. By changing the scale of the wavelet, different time-frequency plot can be generated (Lee and Yamamoto, 1994). With visualization of the signal change and the coefficient generated by different scale, different carbon percentages could possibly be visualized.

Attribute Analysis

Attribute analysis was introduced by the seismic industry whereby they displayed certain functions of the GPR signal reflection and then applied the signal to color rendering (Jol, 2007). Extracting certain features from the received signal, multi-attribute analysis and multi-dimensional attribute analysis provide tools to better interpret 2-D and 3-D GPR data (Marfurt et al., 1998; Schmalz et al., 2002; Gao, 2003; Chopra and Alexeev, 2006; Cassidy, 2007; Wenke Zhao, 2012). An entire data set is called a B-scan, and the columns of the data is called an A-scan. In some cases, an A-scan also is referred to as a trace. Generally, analysis conducted on A-scan wise can be referred as attribute analysis. Some attributes such as instantaneous amplitude, phase, and frequency, were initially used in seismology (Chen and Sidney, 1997; Yilmaz, 2001). Moreover, when applying attribute analysis on GPR data, more attributes such as relative reflectivity, phase relationships, complex trace attributes, and amplitude variation with offset (AVO) are introduced to fit the character of GPR data (Annan, 1993; Chopra and Marfurt, 2007; Morris and Glisic, 2017). Numerous research studies have successfully applied attribute

analysis. However, many of the studies were conducted on relatively homogeneous environments (Falak, 1998; Goodman et al., 1998; Lui and Oristaglio, 1998; De´robert and Abraham, 2000; McClymont et al., 2008; Bradford et al., 2010; Forte et al., 2012). GPR data also can provide some information for material properties like moisture content, and some empirical or theoretical models were previously developed (Brovelli and Cassiani, 1980; Kowalsky et al., 2005; Van Dam, 2014). Attribute analysis is a good quantification method targeting subtle object GPR frequency change such as organic carbon because its size is difficult to visualize using GPR. For this study, maximum amplitude, intensity, energy, and area of the GPR data on A-scan base were chosen to conduct attribute analysis.

Naïve Bayes Predictive Model

Naïve Bayes classifier applies Bayes' theorem with the assumption that all features are strongly independent (McCallum and Nigam, 1998; Rennie et al., 2003). There was some discussion over the assumption of independence, and given that features are computed individually, they should not cause multi-collinearity (McCallum and Nigam, 1998; Rish, 2001). It is a simple probabilistic classifier applied in predictive model or machine learning (Pang et al., 2002). Assigning training and validation data sets, a predictive model could predict soil carbon content using GPR data.

Objectives

Objective 1 Use ground penetrating radar to detect underground biochar amended soil carbon content.

Objective 2 Compare performance of GPR across materials with different structures of carbon.

Objective 3 Compare performance of GPR across different soil moisture levels.

Objective 4 Develop novel GPR analysis methods to quantify carbon.

CHAPTER III

MATERIALS AND METHODS

Material Preparation

Biochar was produced from torrefied napiergrass (*Pennisetum purpureum* Schumach) biomass. Another carbon source was coconut (*Cocos nucifera* L.) shell granular activated carbon (psc 1240, Prominent Systems INC). Activated carbon and graphite were included pure and mixed 1:1 with sand. Biochar: sand treatments were prepared with 8 biochar percentages, 0%, 2%, 4%, 6%, 8%, 10%, 50%, and 100%. Percentages less than 10% were included because they represent approximately the average belowground organic carbon percentages, and 50% and 100% were chosen to compare the GPR performance on aggregated carbon with activated carbon and graphite. Different percentage mixtures were made by mixing the corresponding amount of materials with pure sand by weight and then filling the mixture into sample containers. Each percentage level was called a treatment; therefore, there were 12 treatments in total, including biochar, activated carbon, and graphite. Three replications of each treatment were included.

The sample containers were silicon sandwich bags 19.05 cm x 17.78 cm x 2.54 cm. A hole was punched in the bottom left corner of each bag to allow a 6 cm soft silicon tube to be attached and a silicon ring to secure the tube. This modification provided access to add water without opening the bag multiple times. The volume of the sample container was 580 ml, so different moisture levels could be measured. Adding an additional 58 ml of water created a 10% moisture level, and adding 58 ml more water

creates a 20% moisture level. A water holding capacity experiment was performed to determine the maximum moisture level to be added to all the samples during data collection.

Water Holding Capacity

The water holding capacity experiment used the same material made during material preparation described above. Three replications in completely randomized design were performed. Twelve flasks, 12 Whatman ® filter papers with a 12 cm diameter, and 12 glass funnels were the primary equipment used. The first step was to dampen the folded conical filter paper with distilled water and record the net weight. Next, put the dampen filter paper into the funnel and place the base of the funnel into a flask. Then add approximately 10 g of material on the filter paper-funnel. The last step was to pour 100 ml of distilled water into the funnel and let the water drip for 24 hours. After 24 hours, the total weight of the filter paper, material, and water was determined. Since the filter paper and material weight had been recorded, the amount of water in the material was determined by subtracting the total weight by the previously determined weight of the moistened filter paper and material. The water holding capacity was estimated using the formula:

$$M = W_T - W_P - W_M$$

Where M denotes the water weight held by the material, and W_T denotes the total weight of material, filter paper and water after 24 hours, and W_P denotes the weight of dampen filter paper, and W_M denotes the weight of the dry material. Based on the average water holding capacity of each treatment, moisture levels for testing were determined.

On-Site GPR Data Collection

Data collection was conducted at the Texas A&M University farm on a 20 m x 2.75 m x 1.5 m aboveground trough filled with dry pure garden sand. Three replications were assigned in a randomized complete block design. Every treatment was buried under 100% sand at a depth of 5.08 cm and spaced 25.4 cm apart along a single, medial line in the trough. To investigate radar orientation, two different angles (vertical 0° and off-axis 15°) of seven channels were applied under every moisture level. Each angle was scanned three times. The GPR transmitter frequency was 1.8 GHz. Within the radar antenna were four transmitters and four signal receivers coded into seven channels, and each channel will generate one B scan after one scan. Transmitter 1 and receiver 1 consisted of channel 1, transmitter 2 and receiver 1 consisted of channel 2, transmitter 2 and receiver 2 consisted of channel 3, transmitter 3 and receiver 2 consisted of channel 4, transmitter 3 and receiver 3 consisted of channel 5, transmitter 4 and receiver 3 consisted of channel 6, and transmitter 4 and receiver 4 consisted of channel 7.

Data Analysis

Pre-processing the Data

The raw data filename extension was transferred from private type (.dt) into open source type (.dat) by Matlab® script. Raw data was further transformed into numpy array, which was a grid of stored values, and the data was ready for pre-processing. GPR data pre-processing steps included surface removal, fast forward transfer bandpass filtering, and change the signal into voltage. Surface removal was conducted by implemented Python surface detection function, which removes the noise of the data

above the sand surface, and then subset the bottom of B-scan by adding 50 rows from the sand surface. Bandpass function was conducted after the data passed the surface removal, and the forward transfer bandpass filter set the lower band frequency at 1.0 GHz and higher band frequency at 3.2 GHz. The bandpass filter blocked signals out of the selected frequency range. In this study, the signal returned ranged from 0.9 GHz and 3.6 GHz because the central frequency of the radar was 1.8 GHz. Data signals were further transferred to voltage and then passed through attribute analysis, which was based on analyzing attributes of the entire A-scans.

Wavelet Analysis

The continuous wavelets analysis was conducted on the data. Wavelet analysis was conducted on a script based on Python v. 3.6.5 (Python Software Foundation, 2018), and the script was implemented by research associate Iliyana Debrova. There were 150 scales (from one to 150) that were passed to PyWavelets (Lee et al., 2018) package. Each treatment would have 150 wavelet coefficients corresponding to the 150 scales, and the p-value for each coefficient also was calculated.

Attribute Analysis

After pre-processing, the attribute analysis was performed in a Python script that I developed, and the maximum amplitude, intensity, energy, and area were calculated based on these self-written functions. All of the attributes were transformations of the signals' amplitude on A-scan wise. Maximum amplitude was estimated by finding the maximum value of the A-scan amplitude. Intensity was calculated by finding the maximum value of the squared amplitude on A-scan while energy was computed by

finding the maximum value of the integrated amplitude on A-scan. Lastly, area was estimated by finding the maximum value of the integrated squared amplitude. These estimated values formed a subset with specific A-scans corresponding with the buried treatments.

After completing this workflow, the dataset was exported to spreadsheet for statistical analyses. All statistical analyses were conducted using RStudio v.3.5.2 (RStudio team, 2016).

Statistical Analyses

Differences between the seven channels, antenna angles, moisture levels, and treatments were analyzed based on the attributes. In addition, a naïve Bayes predictive model was trained and validated based on the entire data set. To determine the performance of the seven channels, analysis of variance (ANOVA) was first conducted, then Tukey's HSD test was conducted when the p-value of ANOVA test was significant. The Boxplots of the channels against each attribute was performed to visualize the differences of the seven channels. ANOVA and boxplots were also performed to determine antenna angle difference. The ANOVA and Spearman rank correlation test were performed to obtain the moisture level differences. As for treatment differences, the ANOVA, Tukey's HSD test, and Pearson correlation test were conducted. All analyses were completed on RStudio v.3.5.2, and naïve Bayes predictive model was performed on JMP Pro v. 14.0.0 (SAS Institute, 2019).

CHAPTER IV

RESULTS AND DISCUSSIONS

Water Holding Capacity Experiment

The 12 treatments had variable water holding capacity (Table 1). Only three moisture levels (0%,10%, and 20% percent) were selected because each treatment held different water holding capacity. The 100% biochar held as much as 380% water on average, while 100% graphite held only 10% of water from its weight. With 16.72% and 11.03% water holding capacity at 50% graphite and 100% graphite, respectively, the moisture level of the treatment should not reach over 20%. Thus, only 10% and 20% of moisture level were selected based on the variation of water holding capacity. Adding more water can only cause water sinking under the sample container.

Table 1. Mean water holding capacity of 12 treatments.

Treatment	Replication 1	Replication 2	Replication 3	Mean (%)
0% biochar	9.95%	24.11%	17.34%	17.13%
2% biochar	30.19%	21.42%	39.32%	30.31%
4% biochar	40.81%	40.81%	45.59%	42.40%
6% biochar	36.72%	43.77%	39.77%	40.09%
8% biochar	44.89%	44.47%	46.10%	45.15%
10% biochar	75.51%	62.58%	72.22%	70.10%
50% biochar	211.47%	209.62%	214.63%	211.91%
100% biochar	372.97%	388.53%	384.32%	381.94%
50% activated carbon	82.13%	70.77%	70.10%	74.33%
100% activated carbon	110.17%	113.79%	104.68%	109.55%
50% graphite	20.59%	6.26%	23.31%	16.72%
100% graphite	5.52%	17.51%	10.07%	11.03%

Wavelet Analysis

According to the p-value calculated for each wavelet coefficient, no significant wavelet coefficients were found on the entire data set. This indicates that none of the 150 wavelet length scales were able to match the size of the carbon.

Attribute Analysis

Channel Differences

There were 3,868 samples collected and these were used in the analysis. The ANOVA for four attributes in seven channels showed that, the p-values of their channel means were significantly different (Table 2), which indicates that some channels might

be more useful than other channels. The p-values of ANOVA for all the attributes showed significance, indicating that the attributes have the potential to correlate with carbon content.

Table 2. Summary ANOVA tests across channel for all attributes.

Source		DF	Sum Sq	Mean Sq	F-value	Pr(>F)
Maximum amplitude	Degree	6	130	22	82	3.70e-97***
	Residuals	3900	1000	0.27		
Intensity	Degree	6	160	27	79	6.20e-94***
	Residuals	3900	1300	0.34		
Energy	Degree	6	9300	1600	66	6.50e-78***
	Residuals	3900	92000	24		
Area	Degree	6	5600	930	170	2.40e-192***
	Residuals	3900	21000	5.5		

Note: *, **, and *** denotes significance at 0.05, 0.01, and 0.001 level of probability, respectively.

From the demonstration of the antenna (Figures 1and 2), seven channels were coded and combined by four transmitters and four receivers. The broader channels were closest to the antenna container edge; therefore, the signals were affected the and more signal noise was greater than the middle channels. Outlier count with three interquartile range (Table 3) and boxplots of the attributes distribution across seven channels (Figures 3-6) showed channels 1, 6 and 7 were the poorest performers. Channel 6 data was decided to be kept because it was in the middle of the antenna, so less noise was generated than channel 1 and 7, and exclude another channel would reduce sample size more significantly. Because channel 1 and channel 7 collected less informative data, and their border physical composition, their data were excluded from the entire dataset. All of the following analyses were conducted using only channels 2, 3, 4, 5, and 6.

Table 3. Outlier count with three interquartile range for each antenna channel with all attributes

	Channel1	Channel 2	Channel 3	Channel 4	Channel 5	Channel 6	Channel 7
Maximum Amplitude	0	0	0	0	0	1	0
Intensity	3	0	1	4	3	9	12
Energy	5	1	2	2	4	6	14
Area	1	0	0	0	0	2	2

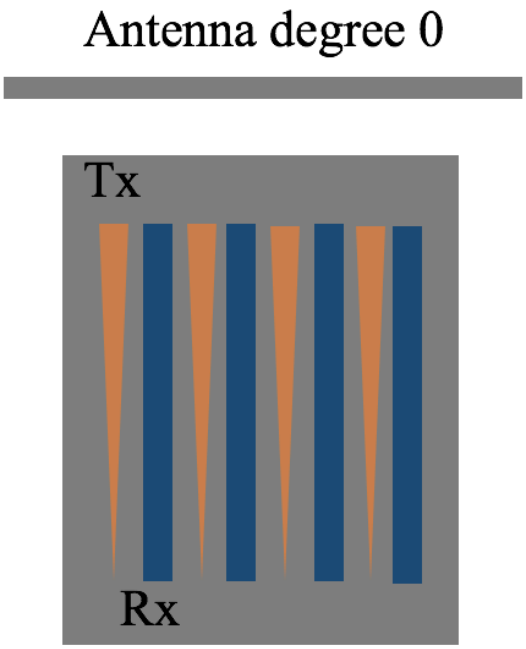

Figure 1. Internal transmitters and receivers of one antenna on degree 0. Orange triangle denotes transmitter; blue rectangle denotes receiver.

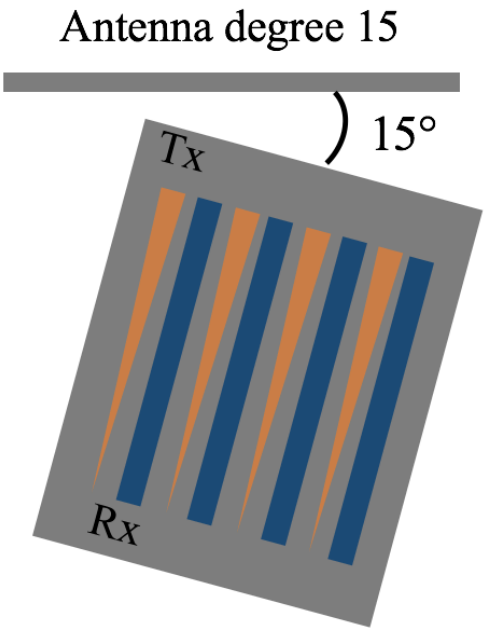

Figure 2. Internal transmitters and receivers of one antenna on degree 15. Orange triangle denotes transmitter; blue rectangle denotes receiver.

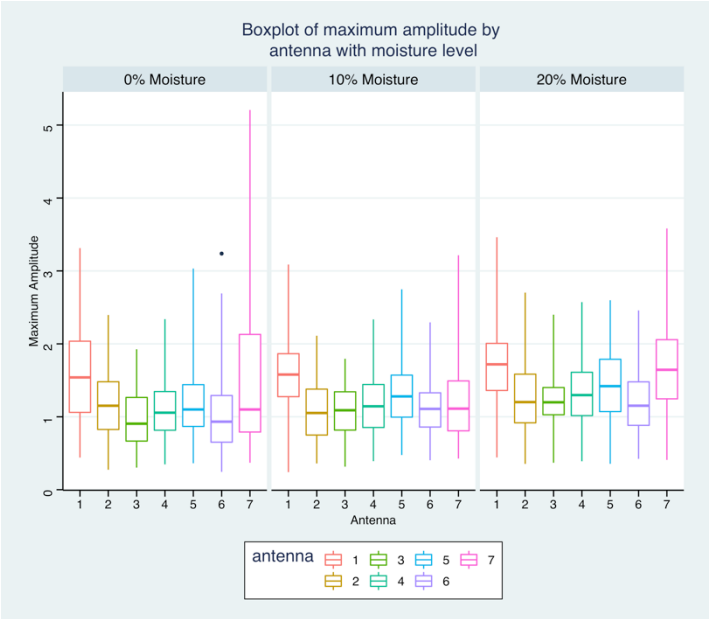

Figure 3. Boxplot of treatment maximum amplitude distribution across seven channels at three moisture levels with three interquartile range.

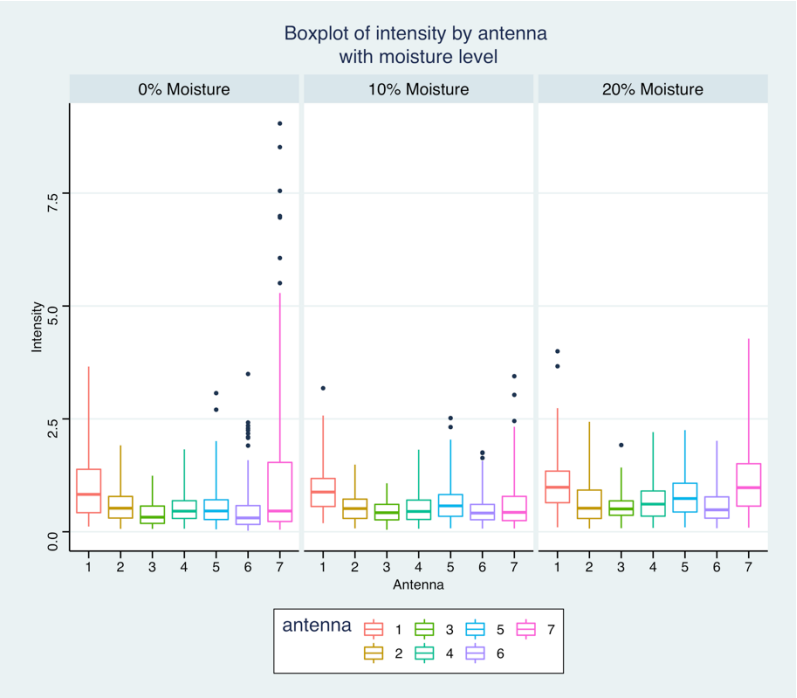

Figure 4. Boxplot of treatment intensity distribution across seven channels at three moisture levels with three interquartile range.

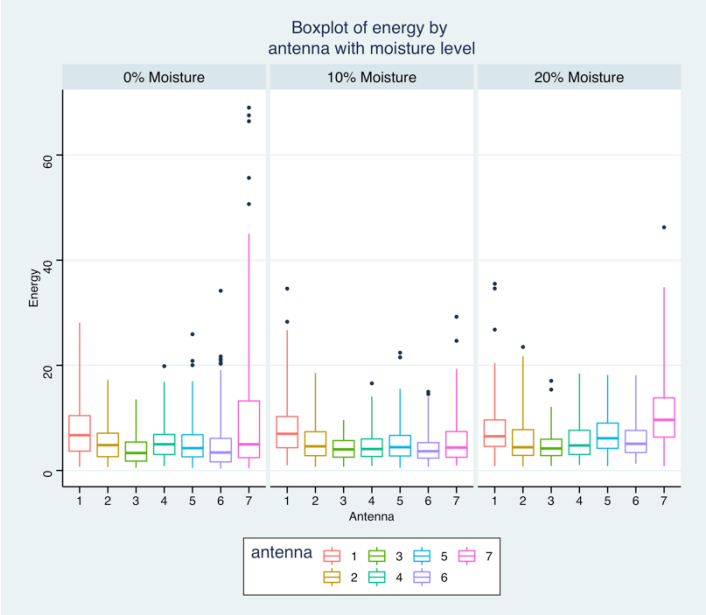

Figure 5. Boxplot of treatment energy distribution across seven channels at three moisture levels with three interquartile range.

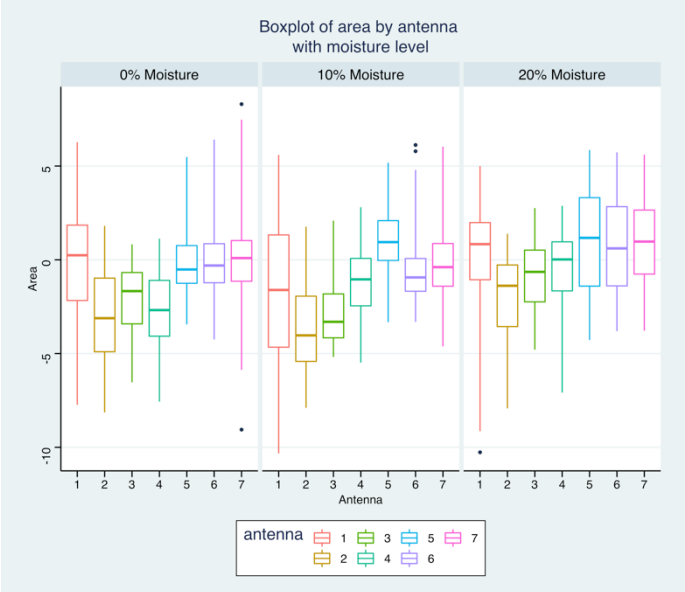

Figure 6. Boxplot of treatment area distribution across seven channels at three moisture levels with three interquartile range.

Antenna Angle

The data sets were divided into two groups. One was collected at degree 0 antenna angle, and the other was collected at the degree 15 antenna angle. Running an ANOVA between the two groups with four attributes individually, maximum amplitude, energy, and intensity showed significant mean differences for antenna angle. Mean difference of treatment area, in contrast, showed no significant differences between the two antenna angles (Table 4).

Table 4. Summary of the ANOVA tests of the mean attribute differences across antennae angle for all attributes.

Source		DF	Sum Sq	Mean Sq	F-value	Pr(>F)
Maximum amplitude	Antenna	1	23	23	120	2.50e-28***
	Residuals	2800	500	0.18		
Intensity	Antenna	1	21	21	150	8.00e-34***
	Residuals	2800	380	0.14		
Energy	Antenna	1	1600	1600	140	2.70e-32***
	Residuals	2800	31000	11		
Area	Antenna	1	10	10	1.7	2.00e-1
	Residuals	2800	17000	6.2		

Note: *, **, and *** denotes significance at 0.05, 0.01, and 0.001 level of probability, respectively.

In the boxplots of the attributes across different antenna angles with three moisture levels (Figures 7-10), showed the maximum amplitude for 0 degree was higher than the degree 15 for all three moisture levels, and intensity and energy showed the same trend. With higher moisture level, the mean maximum amplitude, intensity and energy increased in both angles. In comparing the area under two angles (0° and 15°), at 0% and 10% moisture levels, the mean of the area for degree 15 was higher than the 0 degree and at 20% moisture level, the mean of area for degree 15 was lower than 0 degree. The ANOVA test showed non-significant p-value, indicating that the degree 15 and degree 0 of treatment area were statistically the same. This maybe caused by the nature of the area

since it was calculated by integrating the squared amplitude and the estimated maximum area over the trace.

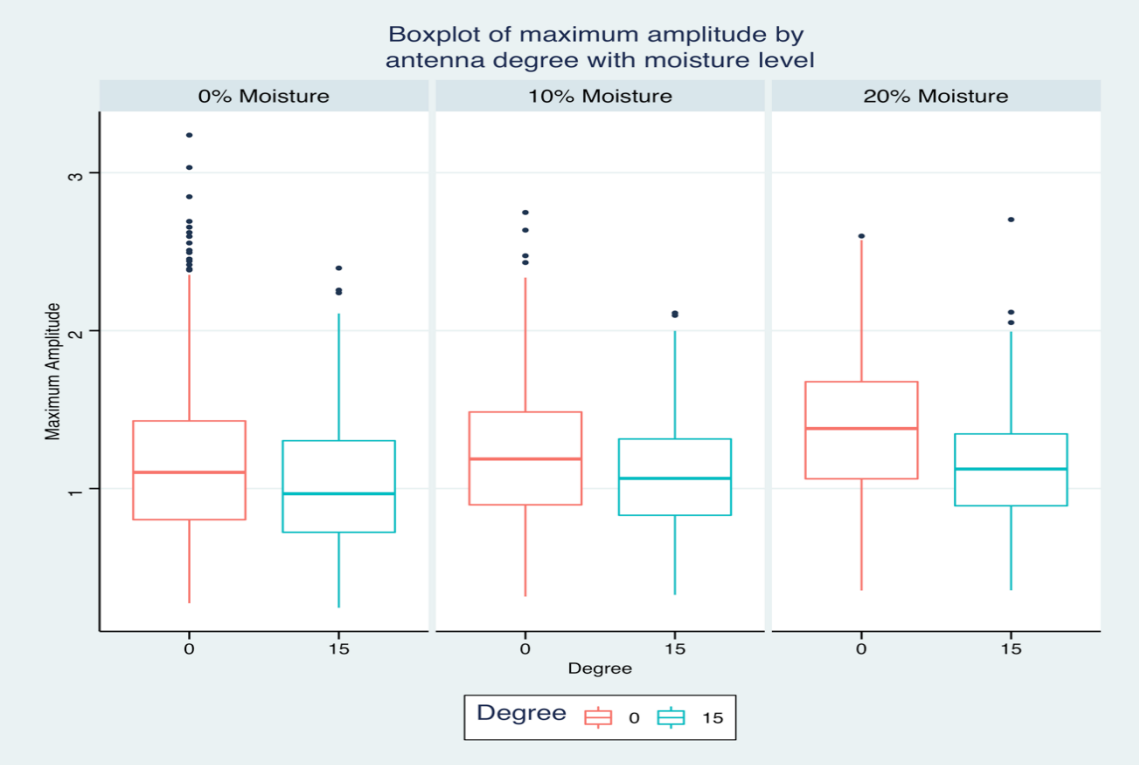

Figure 7. Boxplot of maximum amplitude distribution across 2 antenna angles at three moisture levels.

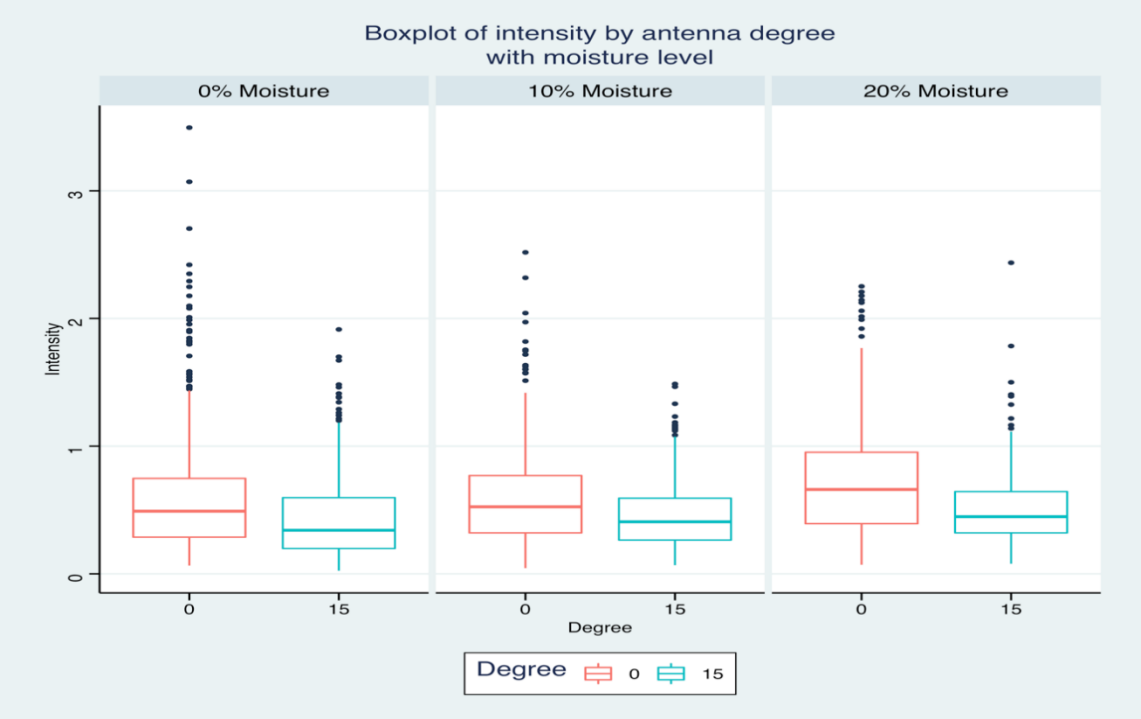

Figure 8. Boxplot of intensity distribution across 2 antenna angles at three moisture levels.

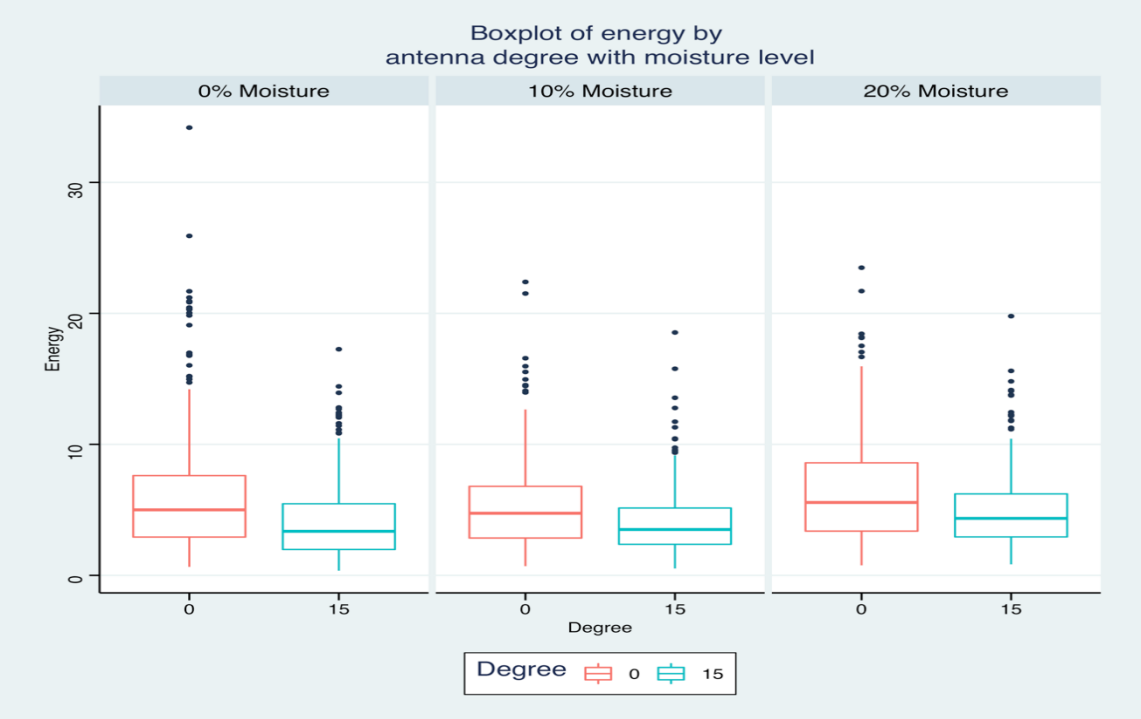

Figure 9. Boxplot of energy distribution across 2 antenna angles at three moisture levels.

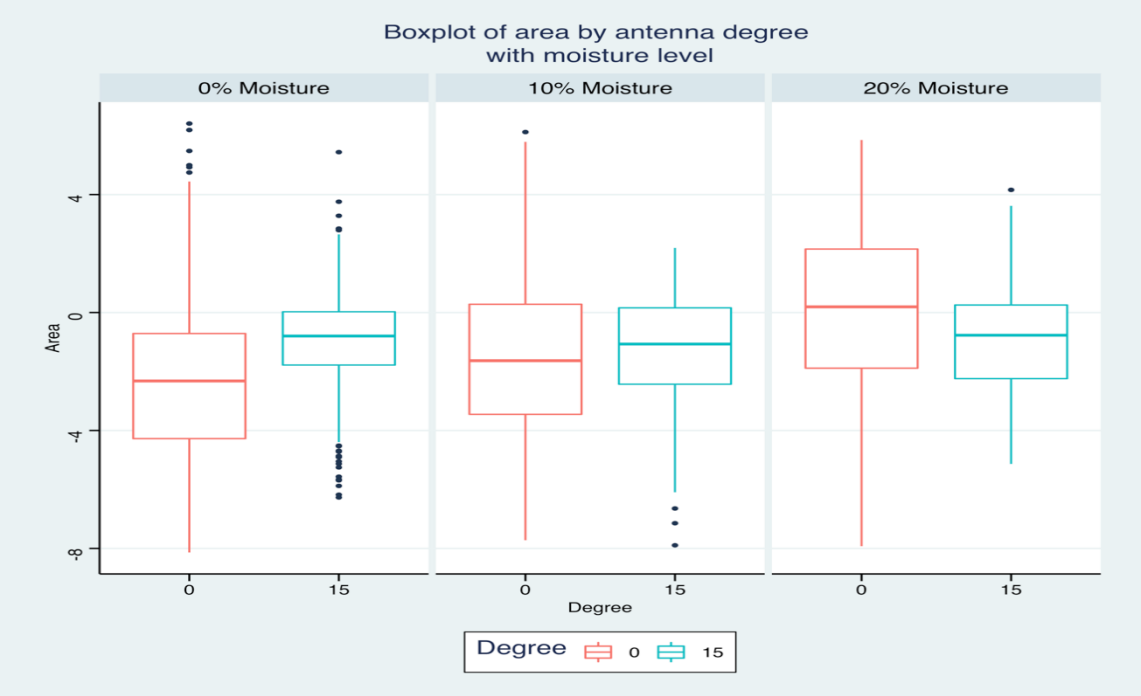

Figure 10. Boxplot of area distribution across 2 antenna angles at three moisture levels.

Moisture Levels

The mean differences for moisture levels were significant (Table 5). This indicates that the variance in the attributes can be used to built a correlation between moisture level and the four attributes individually.

Table 5. Summary of ANOVA tests of the mean attribute differences across moisture levels for all attributes.

Source		DF	Sum Sq	Mean Sq	F-value	Pr(>F)
Maximum amplitude	Moisture	2	17.2	8.581	46.53	<2e-16***
	Residuals	2764	509.8	0.184		
Intensity	Moisture	2	8.7	4.355	30.74	6.28e-14***
	Residuals	2764	391.6	0.142		
Energy	Moisture	2	493	240.60	21.4	5.97e-10***
	Residuals	2764	31846	11.52		
Area	Moisture	2	870	435.1	74.02	<2e-16***
	Residuals	2764	16245	5.9		

Note: *, **, and *** denotes significance at 0.05, 0.01, and 0.001 level of probability, respectively.

Since moisture level was a categorical variable and attributes were continuous variables, Spearman rank correlation analysis was conducted. Spearman rank correlation coefficient assessed the relationship between two variables using a monotonic function. The Spearman correlation plots (Figures 11-14), showed the direction of association between the moisture level and attributes. With a positive correlation coefficient, the attribute increased when the moisture level increased. When the attribute and moisture level associated monotonically, the coefficient became 1. All the coefficients were positive but generally low, and all the p-values were significant. The correlation coefficients were low because the data was derived from 12 treatments for each moisture level. The upper bar plot was the distribution of moisture levels, and the bar plot on the right is the distribution of the attributes. Therefore, for all attributes, they increased when the moisture level increased, which indicates that GPR is performing better at a higher moisture level. This can be explained by carbon aggregation. Since water and carbon

aggregates, the target object became larger at higher moisture level, which made it easier for GPR to detect.

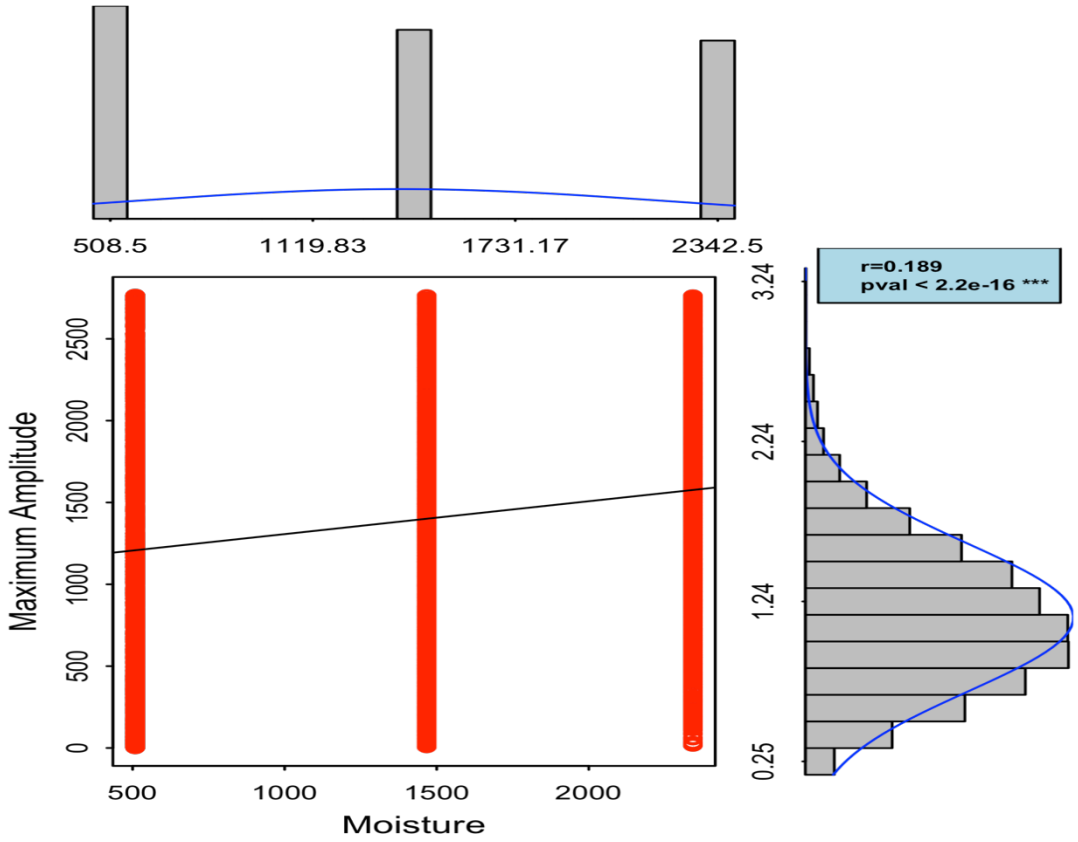

Figure 11. Spearman correlation plot of treatment moisture level with maximum amplitude.

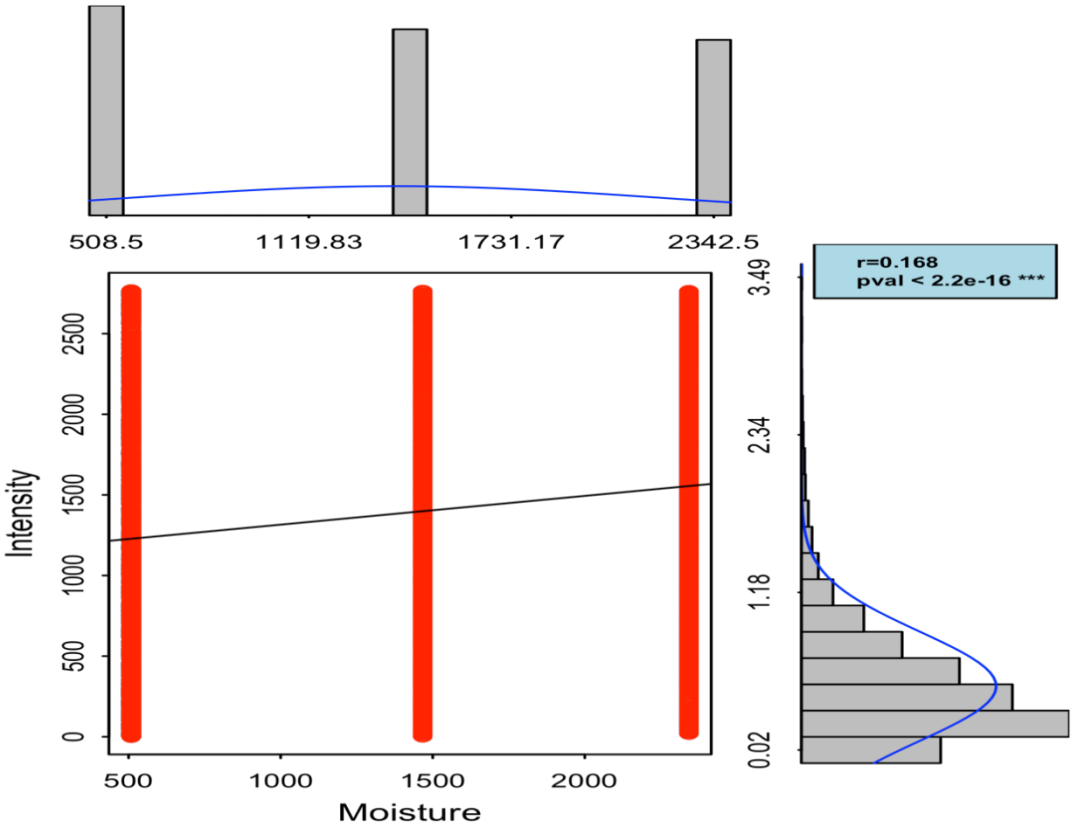

Figure 12. Spearman correlation plot of treatment moisture level with intensity.

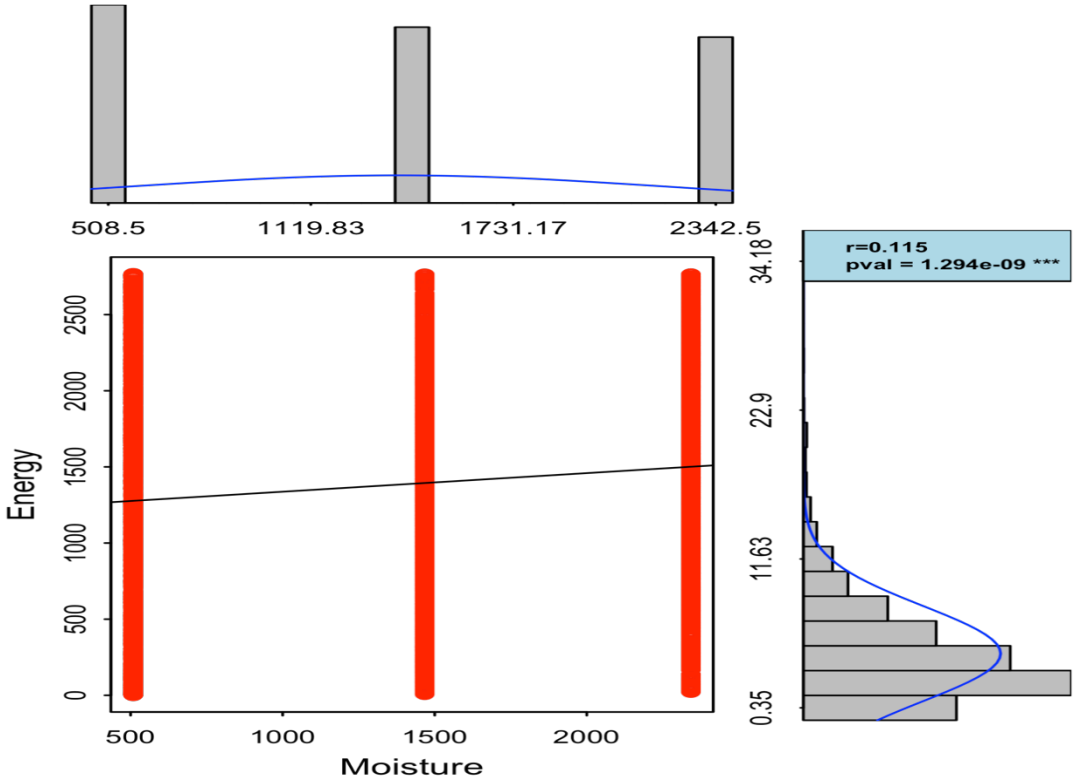

Figure 13. Spearman correlation plot of treatment moisture level with energy.

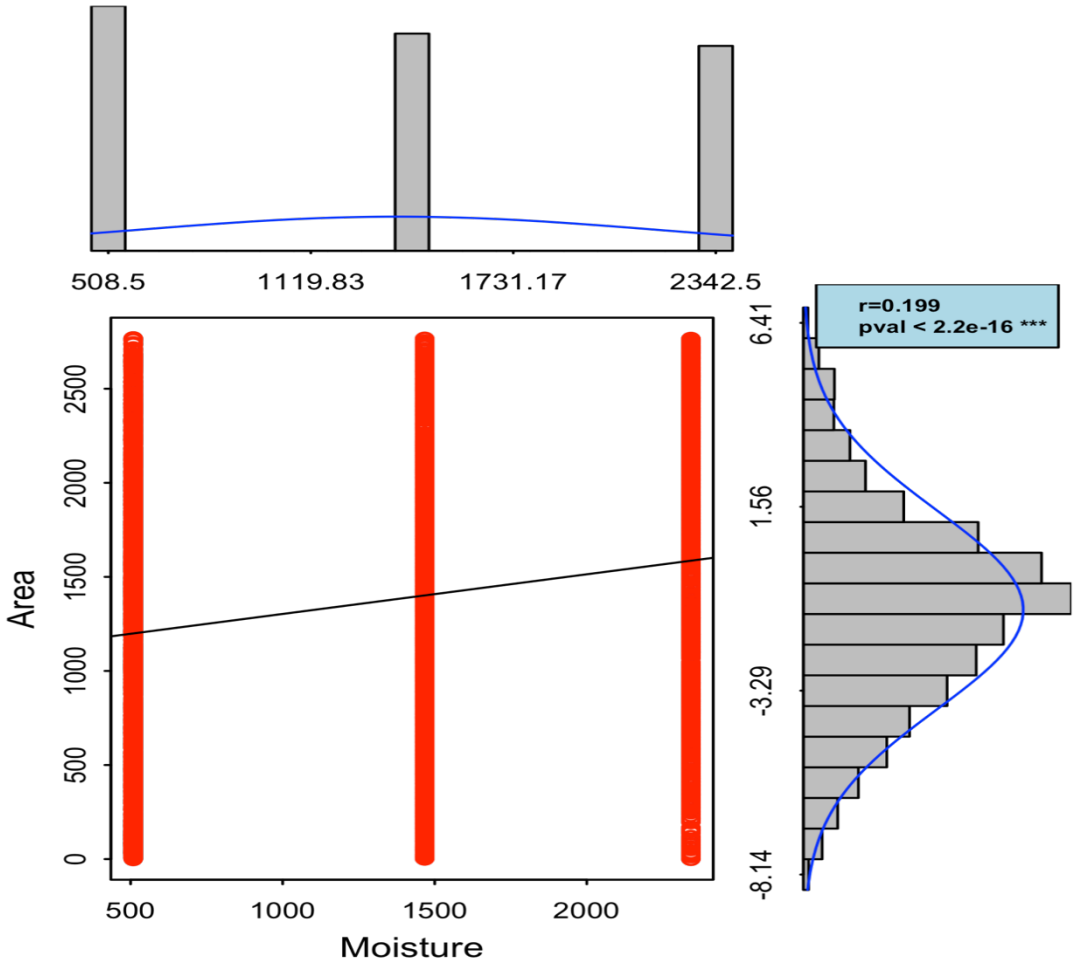

Figure 14. Spearman correlation plot of treatment moisture level with area.

Treatment Differences

All the treatments represented different percentages of carbon. It has 55%, 100%, and 80% carbon for pure biochar, pure graphite, and activated carbon, respectively. There were significant differences in the ANOVA tests for all the attributes across all the treatments (Table 6). Pearson correlation analysis indicated very limited relationships between treatments and attributes.

Table 6. Summary of the ANOVA tests of the mean attribute differences across treatments for all attributes.

Source		DF	Sum Sq	Mean Sq	F-value	Pr(>F)
Maximum amplitude	Treatments	11	37.6	3.419	19.25	<2e-16***
	Residuals	2755	489.3	0.178		
Intensity	Treatments	11	26.4	2.3996	17.68	<2e-16***
	Residuals	2755	373.9	0.1357		
Energy	Treatments	11	2894	263.13	24.62	<2e-16***
	Residuals	2755	29445	10.69		
Area	Treatments	11	1471	133.74	23.55	<2e-16***
	Residuals	2755	15644	5.68		

Note: *, **, and *** denotes significance at 0.05, 0.01, and 0.001 level of probability, respectively.

The correlation coefficients between attributes and all treatments were non-significant except for area (Table 7) which had a negative correlation coefficient of -0.0815. This indicated the area decreased when the carbon content increased., This correlation is very small, but sub-group, the treatment might return higher correlation.

Table 7. Pearson correlation coefficient between attributes and all treatments.

	Pearson correlation coefficient	P-value
Maximum amplitude	-0.0121	0.5238
Intensity	-0.0063	0.7407
Energy	0.0140	0.4628
Area	-0.0815	1.79e-05***

Note: *, **, and *** denotes significance at 0.05, 0.01, and 0.001 level of probability, respectively.

To determine which mean treatment was significantly different from another treatment, Tukey's HSD test was completed (Tables 8-11). Distinct groupings were noted in the series of tables. For example, 50% and 100% graphite, and pure sand were grouped together for all the attributes. For maximum amplitude, 50% and 100%

activated carbon, and 2%, 6%, 8%, and 50% biochar were grouped while for intensity, 50% and 100% activated carbon, and 2%, 6%, 8%, and 50% biochar were grouped. For energy, 50% and 100% activated carbon and 2% and 50% biochar were grouped. For area, 50% and100% activated carbon and 2%, 6%, 8%, 50%, and 100% biochar were grouped. Moreover, 50% and 100% activated carbon with pure sand were grouped and all percentages of biochar with pure sand were grouped as well.

Table 8. Tukey's HSD test results for maximum amplitude across each treatment.

Ordered Differences Report

Level	- Level	Difference	Std Err Dif	Lower CL	Upper CL	p-Value
8% Biochar	10% Biochar	0.3816293	0.0424364	0.242827	0.5204320	<.0001*
8% Biochar	0% Biochar	0.3590647	0.0381555	0.234264	0.4838654	<.0001*
8% Biochar	100% Activated C	0.3260215	0.0381169	0.201347	0.4506958	<.0001*
8% Biochar	50% Activated C	0.3060849	0.0383129	0.180770	0.4314003	<.0001*
100% Graphite	10% Biochar	0.3040194	0.0424011	0.165332	0.4427065	<.0001*
2% Biochar	10% Biochar	0.2870420	0.0423312	0.148583	0.4255007	<.0001*
100% Graphite	0% Biochar	0.2814548	0.0381162	0.156783	0.4061270	<.0001*
2% Biochar	0% Biochar	0.2644774	0.0380385	0.140059	0.3888955	<.0001*
50% Biochar	10% Biochar	0.2635385	0.0425078	0.124502	0.4025747	<.0001*
8% Biochar	100% Biochar	0.2629401	0.0381555	0.138139	0.3877408	<.0001*
8% Biochar	50% Graphite	0.2497421	0.0382336	0.124686	0.3747983	<.0001*
100% Graphite	100% Activated C	0.2484116	0.0380776	0.123866	0.3729573	<.0001*
50% Biochar	0% Biochar	0.2409739	0.0382349	0.115914	0.3660343	<.0001*
2% Biochar	100% Activated C	0.2314342	0.0379998	0.107143	0.3557255	<.0001*
100% Graphite	50% Activated C	0.2284750	0.0382738	0.103288	0.3536624	<.0001*
6% Biochar	10% Biochar	0.2183940	0.0464712	0.066394	0.3703939	0.0002*
8% Biochar	4% Biochar	0.2133883	0.0381944	0.088460	0.3383163	<.0001*
2% Biochar	50% Activated C	0.2114976	0.0381964	0.086563	0.3364319	<.0001*
50% Biochar	100% Activated C	0.2079307	0.0381964	0.082996	0.3328650	<.0001*
6% Biochar	0% Biochar	0.1958294	0.0425978	0.056499	0.3351600	0.0003*
50% Biochar	50% Activated C	0.1879941	0.0383919	0.062420	0.3135682	<.0001*
100% Graphite	100% Biochar	0.1853301	0.0381162	0.060658	0.3100024	<.0001*
100% Graphite	50% Graphite	0.1721322	0.0381944	0.047204	0.2970602	0.0004*
2% Biochar	100% Biochar	0.1683528	0.0380385	0.043935	0.2927708	0.0006*
4% Biochar	10% Biochar	0.1682410	0.0424011	0.029554	0.3069282	0.0043*
8% Biochar	6% Biochar	0.1632354	0.0426677	0.023676	0.3027948	0.0074*
6% Biochar	100% Activated C	0.1627861	0.0425632	0.023569	0.3020036	0.0074*
2% Biochar	50% Graphite	0.1551548	0.0381169	0.030480	0.2798291	0.0028*
4% Biochar	0% Biochar	0.1456764	0.0381162	0.021004	0.2703486	0.0075*
50% Biochar	100% Biochar	0.1448493	0.0382349	0.019789	0.2699097	0.0085*
6% Biochar	50% Activated C	0.1428496	0.0427388	0.003058	0.2826414	0.0400*
100% Graphite	4% Biochar	0.1357784	0.0381552	0.010979	0.2605780	0.0195*
50% Graphite	10% Biochar	0.1318872	0.0424364	-0.006915	0.2706898	0.0809
50% Biochar	50% Graphite	0.1316513	0.0383129	0.006336	0.2569667	0.0295*
2% Biochar	4% Biochar	0.1188010	0.0380776	-0.005745	0.2433467	0.0782
100% Biochar	10% Biochar	0.1186892	0.0423660	-0.019883	0.2572618	0.1797
8% Biochar	50% Biochar	0.1180908	0.0383129	-0.007225	0.2434062	0.0870
4% Biochar	100% Activated C	0.1126332	0.0380776	-0.011913	0.2371789	0.1218
50% Graphite	0% Biochar	0.1093226	0.0381555	-0.015478	0.2341233	0.1541
6% Biochar	100% Biochar	0.0997047	0.0425978	-0.039626	0.2390353	0.4477
100% Biochar	0% Biochar	0.0961246	0.0380773	-0.028420	0.2206693	0.3249
50% Biochar	4% Biochar	0.0952975	0.0382738	-0.029890	0.2204849	0.3466
8% Biochar	2% Biochar	0.0945873	0.0381169	-0.030087	0.2192616	0.3520
4% Biochar	50% Activated C	0.0926966	0.0382738	-0.032491	0.2178841	0.3913
6% Biochar	50% Graphite	0.0865068	0.0426677	-0.053053	0.2260663	0.6746
100% Graphite	6% Biochar	0.0856254	0.0426326	-0.053819	0.2250700	0.6878
8% Biochar	100% Graphite	0.0776099	0.0381944	-0.047318	0.2025379	0.6714
50% Graphite	100% Activated C	0.0762794	0.0381169	-0.048395	0.2009537	0.6928
50% Activated C	10% Biochar	0.0755444	0.0425078	-0.063492	0.2145806	0.8306
2% Biochar	6% Biochar	0.0686480	0.0425632	-0.070569	0.2078655	0.9047
100% Biochar	100% Activated C	0.0630814	0.0380385	-0.061337	0.1874995	0.8867
50% Graphite	50% Activated C	0.0563428	0.0383129	-0.068973	0.1816582	0.9485
100% Activated C	10% Biochar	0.0556078	0.0423312	-0.082851	0.1940665	0.9775
50% Activated C	0% Biochar	0.0529798	0.0382349	-0.072081	0.1780402	0.9664
6% Biochar	4% Biochar	0.0501529	0.0426326	-0.089292	0.1895976	0.9907
4% Biochar	100% Biochar	0.0495518	0.0381162	-0.075120	0.1742240	0.9793
50% Biochar	6% Biochar	0.0451446	0.0427388	-0.094647	0.1849363	0.9963
100% Biochar	50% Activated C	0.0431449	0.0382349	-0.081916	0.1682053	0.9934
100% Graphite	50% Biochar	0.0404809	0.0382738	-0.084707	0.1656683	0.9962
4% Biochar	50% Graphite	0.0363538	0.0381944	-0.088574	0.1612818	0.9985
100% Activated C	0% Biochar	0.0330432	0.0380385	-0.091375	0.1574613	0.9994
2% Biochar	50% Biochar	0.0235035	0.0381964	-0.101431	0.1484378	1.0000
0% Biochar	10% Biochar	0.0225646	0.0423660	-0.116008	0.1611371	1.0000
50% Activated C	100% Activated C	0.0199366	0.0381964	-0.104998	0.1448709	1.0000
100% Graphite	2% Biochar	0.0169774	0.0380776	-0.107568	0.1415231	1.0000
50% Graphite	100% Biochar	0.0131979	0.0381555	-0.111603	0.1379986	1.0000

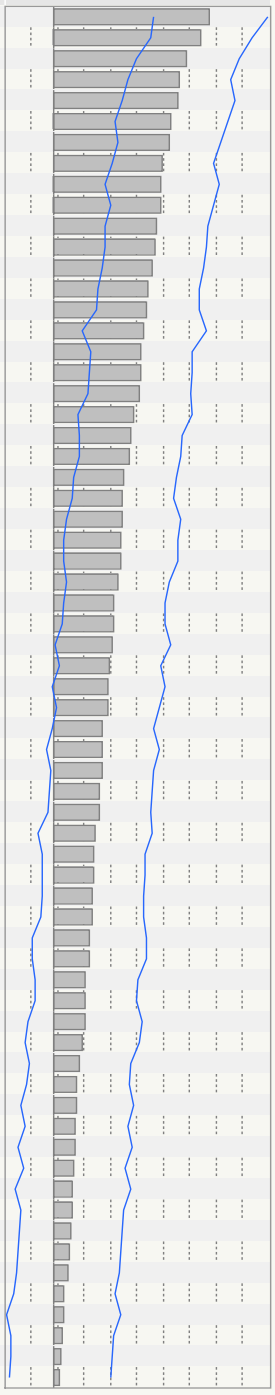

Table 9. Tukey's HSD test results for intensity across each treatment.

Ordered Differences Report

Level	- Level	Difference	Std Err Dif	Lower CL	Upper CL	p-Value
8% Biochar	10% Biochar	0.3290276	0.0370962	0.207692	0.4503634	<.0001*
8% Biochar	0% Biochar	0.3150763	0.0333540	0.205980	0.4241721	<.0001*
8% Biochar	50% Activated C	0.2751570	0.0334916	0.165611	0.3847027	<.0001*
8% Biochar	100% Activated C	0.2598785	0.0333203	0.150893	0.3688638	<.0001*
100% Graphite	10% Biochar	0.2457353	0.0370653	0.124500	0.3669701	<.0001*
2% Biochar	10% Biochar	0.2411895	0.0370043	0.120154	0.3622246	<.0001*
8% Biochar	100% Biochar	0.2330821	0.0333540	0.123986	0.3421779	<.0001*
100% Graphite	0% Biochar	0.2317839	0.0333197	0.122800	0.3407675	<.0001*
2% Biochar	0% Biochar	0.2272382	0.0332518	0.118477	0.3359995	<.0001*
50% Biochar	10% Biochar	0.2195225	0.0371586	0.097983	0.3410624	<.0001*
50% Biochar	0% Biochar	0.2055711	0.0334235	0.096248	0.3148940	<.0001*
8% Biochar	50% Graphite	0.2019872	0.0334223	0.092668	0.3113064	<.0001*
8% Biochar	4% Biochar	0.1975735	0.0333881	0.088366	0.3067806	<.0001*
100% Graphite	50% Activated C	0.1918647	0.0334574	0.082431	0.3012986	<.0001*
2% Biochar	50% Activated C	0.1873189	0.0333898	0.078106	0.2965315	<.0001*
6% Biochar	10% Biochar	0.1840609	0.0406233	0.051189	0.3169333	0.0004*
100% Graphite	100% Activated C	0.1765861	0.0332859	0.067713	0.2854591	<.0001*
2% Biochar	100% Activated C	0.1720403	0.0332179	0.063390	0.2806909	<.0001*
6% Biochar	0% Biochar	0.1701096	0.0372373	0.048312	0.2919069	0.0003*
50% Biochar	50% Activated C	0.1656519	0.0335607	0.055880	0.2754237	<.0001*
50% Biochar	100% Activated C	0.1503733	0.0333898	0.041161	0.2595859	0.0004*
100% Graphite	100% Biochar	0.1497898	0.0333197	0.040806	0.2587733	0.0004*
2% Biochar	100% Biochar	0.1452440	0.0332518	0.036483	0.2540054	0.0008*
8% Biochar	6% Biochar	0.1449667	0.0372985	0.022969	0.2669641	0.0059*
4% Biochar	10% Biochar	0.1314541	0.0370653	0.010219	0.2526889	0.0203*
6% Biochar	50% Activated C	0.1301903	0.0373605	0.007990	0.2523908	0.0251*
50% Graphite	10% Biochar	0.1270404	0.0370962	0.005705	0.2483762	0.0307*
50% Biochar	100% Biochar	0.1235770	0.0334235	0.014254	0.2328998	0.0119*
100% Graphite	50% Graphite	0.1186949	0.0333881	0.009488	0.2279020	0.0198*
4% Biochar	0% Biochar	0.1175028	0.0333197	0.008519	0.2264863	0.0218*
6% Biochar	100% Activated C	0.1149118	0.0372070	-0.006787	0.2366101	0.0855
100% Graphite	4% Biochar	0.1142812	0.0333538	0.005186	0.2233761	0.0305*
2% Biochar	50% Graphite	0.1141491	0.0333203	0.005164	0.2231345	0.0305*
50% Graphite	0% Biochar	0.1130890	0.0333540	0.003993	0.2221849	0.0343*
2% Biochar	4% Biochar	0.1097354	0.0332859	0.000862	0.2186084	0.0462*
8% Biochar	50% Biochar	0.1095051	0.0334916	-0.000041	0.2190509	0.0502
100% Biochar	10% Biochar	0.0959455	0.0370347	-0.025189	0.2170801	0.2853
50% Biochar	50% Graphite	0.0924821	0.0334916	-0.017064	0.2020278	0.1974
6% Biochar	100% Biochar	0.0881154	0.0372373	-0.033682	0.2099127	0.4296
50% Biochar	4% Biochar	0.0880684	0.0334574	-0.021366	0.1975023	0.2620
8% Biochar	2% Biochar	0.0878381	0.0333203	-0.021147	0.1968235	0.2598
8% Biochar	100% Graphite	0.0832923	0.0333881	-0.025915	0.1924994	0.3435
100% Biochar	0% Biochar	0.0819942	0.0332856	-0.026878	0.1908662	0.3638
4% Biochar	50% Activated C	0.0775835	0.0334574	-0.031850	0.1870174	0.4632
50% Graphite	50% Activated C	0.0731698	0.0334916	-0.036376	0.1827155	0.5610
100% Activated C	10% Biochar	0.0691492	0.0370043	-0.051886	0.1901843	0.7787
4% Biochar	100% Activated C	0.0623049	0.0332859	-0.046568	0.1711779	0.7768
100% Graphite	6% Biochar	0.0616743	0.0372678	-0.060223	0.1835713	0.8882
50% Graphite	100% Activated C	0.0578912	0.0333203	-0.051094	0.1668766	0.8508
2% Biochar	6% Biochar	0.0571286	0.0372070	-0.064570	0.1788269	0.9308
6% Biochar	50% Graphite	0.0570205	0.0372985	-0.064977	0.1790179	0.9328
100% Activated C	0% Biochar	0.0551978	0.0332518	-0.053564	0.1639592	0.8860
50% Activated C	10% Biochar	0.0538706	0.0371586	-0.067669	0.1754106	0.9534
6% Biochar	4% Biochar	0.0526068	0.0372678	-0.069290	0.1745038	0.9615
100% Biochar	50% Activated C	0.0420749	0.0334235	-0.067248	0.1513978	0.9839
50% Activated C	0% Biochar	0.0399193	0.0334235	-0.069404	0.1492421	0.9895
4% Biochar	100% Biochar	0.0355086	0.0333197	-0.073475	0.1444921	0.9960
50% Biochar	6% Biochar	0.0354615	0.0373605	-0.086739	0.1576620	0.9986
50% Graphite	100% Biochar	0.0310949	0.0333540	-0.078001	0.1401907	0.9988
100% Biochar	100% Activated C	0.0267963	0.0332518	-0.081965	0.1355577	0.9997
100% Graphite	50% Biochar	0.0262128	0.0334574	-0.083221	0.1356467	0.9998
2% Biochar	50% Biochar	0.0216670	0.0333898	-0.087546	0.1308796	1.0000
100% Activated C	50% Activated C	0.0152785	0.0333898	-0.093934	0.1244912	1.0000
0% Biochar	10% Biochar	0.0139513	0.0370347	-0.107183	0.1350860	1.0000
100% Graphite	2% Biochar	0.0045458	0.0332859	-0.104327	0.1134187	1.0000
4% Biochar	50% Graphite	0.0044137	0.0333881	-0.104793	0.1136208	1.0000

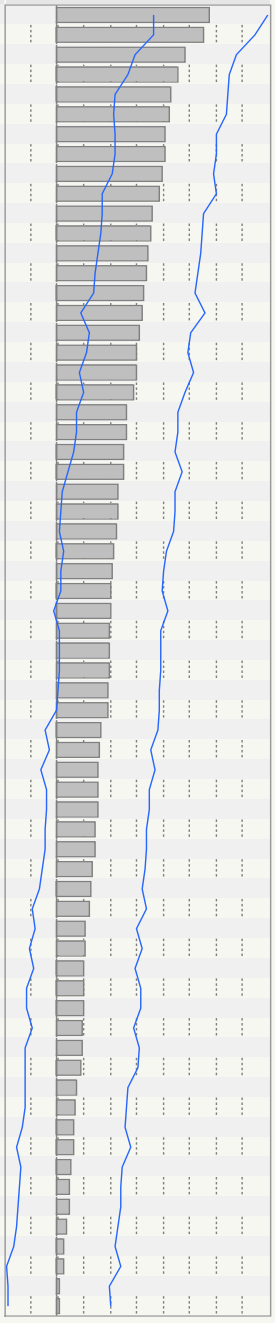

Table 10. Tukey's HSD test results for energy across each treatment.

Ordered Differences Report

Level	- Level	Difference	Std Err Dif	Lower CL	Upper CL	p-Value
8% Biochar	10% Biochar	3.492827	0.3291903	2.41610	4.569557	<.0001*
8% Biochar	0% Biochar	3.268876	0.2959827	2.30076	4.236989	<.0001*
8% Biochar	50% Activated C	3.036593	0.2972033	2.06449	4.008698	<.0001*
8% Biochar	100% Activated C	2.859006	0.2956830	1.89187	3.826138	<.0001*
100% Graphite	10% Biochar	2.822861	0.3289164	1.74703	3.898694	<.0001*
100% Graphite	0% Biochar	2.598909	0.2956780	1.63179	3.566026	<.0001*
2% Biochar	10% Biochar	2.437171	0.3283746	1.36311	3.511233	<.0001*
100% Graphite	50% Activated C	2.366626	0.2968999	1.39551	3.337739	<.0001*
8% Biochar	100% Biochar	2.238717	0.2959827	1.27060	3.206830	<.0001*
2% Biochar	0% Biochar	2.213220	0.2950752	1.24808	3.178365	<.0001*
8% Biochar	50% Graphite	2.195800	0.2965886	1.22571	3.165894	<.0001*
100% Graphite	100% Activated C	2.189039	0.2953780	1.22290	3.155174	<.0001*
8% Biochar	6% Biochar	2.133296	0.3309852	1.05070	3.215896	<.0001*
8% Biochar	4% Biochar	2.076034	0.2962845	1.10693	3.045134	<.0001*
2% Biochar	50% Activated C	1.980937	0.2962995	1.01179	2.950086	<.0001*
50% Biochar	10% Biochar	1.896281	0.3297442	0.81774	2.974823	<.0001*
2% Biochar	100% Activated C	1.803350	0.2947746	0.83919	2.767511	<.0001*
50% Biochar	0% Biochar	1.672330	0.2965986	0.70220	2.642458	<.0001*
8% Biochar	50% Biochar	1.596546	0.2972033	0.62444	2.568651	<.0001*
100% Graphite	100% Biochar	1.568750	0.2956780	0.60163	2.535867	<.0001*
100% Graphite	50% Graphite	1.525833	0.2962845	0.55673	2.494933	<.0001*
100% Graphite	6% Biochar	1.463329	0.3307128	0.38162	2.545038	0.0006*
50% Biochar	50% Activated C	1.440047	0.2978167	0.46594	2.414159	<.0001*
4% Biochar	10% Biochar	1.416793	0.3289164	0.34096	2.492627	0.0010*
100% Graphite	4% Biochar	1.406067	0.2959802	0.43796	2.374172	0.0001*
6% Biochar	10% Biochar	1.359532	0.3604895	0.18043	2.538636	0.0091*
50% Graphite	10% Biochar	1.297028	0.3291903	0.22030	2.373757	0.0048*
50% Biochar	100% Activated C	1.262460	0.2962995	0.29331	2.231609	0.0013*
100% Biochar	10% Biochar	1.254110	0.3286445	0.17917	2.329055	0.0077*
4% Biochar	0% Biochar	1.192842	0.2956780	0.22573	2.159958	0.0033*
2% Biochar	100% Biochar	1.183061	0.2950752	0.21792	2.148206	0.0036*
2% Biochar	50% Graphite	1.140144	0.2956830	0.17301	2.107276	0.0066*
6% Biochar	0% Biochar	1.135580	0.3304424	0.05476	2.216406	0.0295*
2% Biochar	6% Biochar	1.077640	0.3301740	-0.00231	2.157587	0.0511
50% Graphite	0% Biochar	1.073076	0.2959827	0.10496	2.041189	0.0154*
8% Biochar	2% Biochar	1.055656	0.2956830	0.08852	2.022789	0.0187*
100% Biochar	0% Biochar	1.030159	0.2953755	0.06403	1.996286	0.0249*
2% Biochar	4% Biochar	1.020378	0.2953780	0.05424	1.986513	0.0278*
4% Biochar	50% Activated C	0.960559	0.2968999	-0.01055	1.931672	0.0557
100% Graphite	50% Biochar	0.926579	0.2968999	-0.04453	1.897692	0.0780
6% Biochar	50% Activated C	0.903297	0.3315362	-0.18111	1.987700	0.2145
50% Graphite	50% Activated C	0.840793	0.2972033	-0.13131	1.812898	0.1683
100% Biochar	50% Activated C	0.797876	0.2965986	-0.17225	1.768003	0.2316
4% Biochar	100% Activated C	0.782972	0.2953780	-0.18316	1.749107	0.2520
6% Biochar	100% Activated C	0.725710	0.3301740	-0.35424	1.805657	0.5512
8% Biochar	100% Graphite	0.669967	0.2962845	-0.29913	1.639067	0.5049
50% Graphite	100% Activated C	0.663206	0.2956830	-0.30393	1.630339	0.5182
50% Biochar	100% Biochar	0.642171	0.2965986	-0.32796	1.612299	0.5754
100% Activated C	10% Biochar	0.633821	0.3283746	-0.44024	1.707883	0.7402
100% Biochar	100% Activated C	0.620289	0.2950752	-0.34486	1.585433	0.6213
50% Biochar	50% Graphite	0.599254	0.2972033	-0.37285	1.571359	0.6823
2% Biochar	50% Biochar	0.540890	0.2962995	-0.42826	1.510039	0.8041
50% Biochar	6% Biochar	0.536750	0.3315362	-0.54765	1.621152	0.9024
50% Biochar	4% Biochar	0.479488	0.2968999	-0.49162	1.450601	0.9039
50% Activated C	10% Biochar	0.456234	0.3297442	-0.62231	1.534776	0.9667
100% Activated C	0% Biochar	0.409870	0.2950752	-0.55527	1.375015	0.9658
100% Graphite	2% Biochar	0.385689	0.2953780	-0.58045	1.351824	0.9785
50% Activated C	0% Biochar	0.232283	0.2965986	-0.73784	1.202410	0.9998
0% Biochar	10% Biochar	0.223951	0.3286445	-0.85099	1.298896	0.9999
100% Activated C	50% Activated C	0.177587	0.2962995	-0.79156	1.146736	1.0000
4% Biochar	100% Biochar	0.162683	0.2956780	-0.80443	1.129799	1.0000
4% Biochar	50% Graphite	0.119766	0.2962845	-0.84933	1.088866	1.0000
6% Biochar	100% Biochar	0.105421	0.3304424	-0.97540	1.186247	1.0000
6% Biochar	50% Graphite	0.062504	0.3309852	-1.02010	1.145105	1.0000
4% Biochar	6% Biochar	0.057261	0.3307128	-1.02445	1.138971	1.0000
50% Graphite	100% Biochar	0.042917	0.2959827	-0.92520	1.011030	1.0000

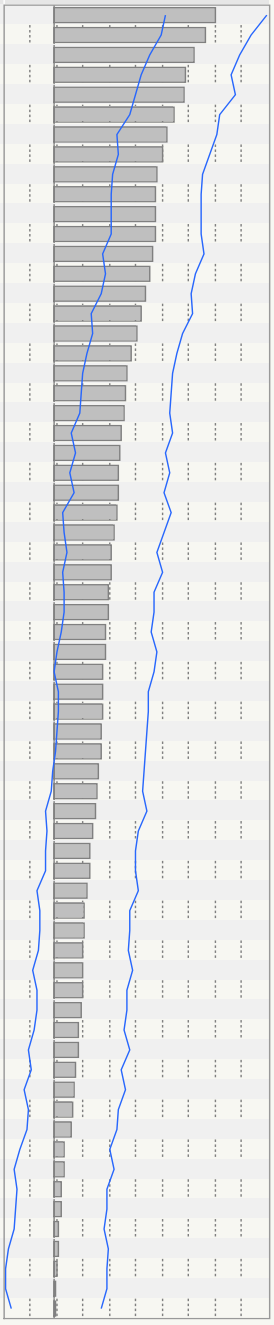

Table 11. Tukey's HSD test results for area across each treatment.

Ordered Differences Report

Level	- Level	Difference	Std Err Dif	Lower CL	Upper CL	p-Value
0% Biochar	100% Graphite	2.301760	0.2155219	1.59682	3.006698	<.0001*
50% Graphite	100% Graphite	2.115780	0.2159640	1.40940	2.822165	<.0001*
50% Activated C	100% Graphite	2.097252	0.2164125	1.38940	2.805104	<.0001*
0% Biochar	8% Biochar	2.019861	0.2157440	1.31420	2.725526	<.0001*
50% Graphite	8% Biochar	1.833882	0.2161856	1.12677	2.540991	<.0001*
50% Activated C	8% Biochar	1.815354	0.2166337	1.10678	2.523928	<.0001*
10% Biochar	100% Graphite	1.795064	0.2397496	1.01088	2.579247	<.0001*
100% Activated C	100% Graphite	1.709037	0.2153032	1.00481	2.413260	<.0001*
0% Biochar	100% Biochar	1.696579	0.2153014	0.99236	2.400796	<.0001*
4% Biochar	100% Graphite	1.624045	0.2157422	0.91839	2.329704	<.0001*
10% Biochar	8% Biochar	1.513165	0.2399493	0.72833	2.298002	<.0001*
50% Graphite	100% Biochar	1.510600	0.2157440	0.80494	2.216264	<.0001*
50% Activated C	100% Biochar	1.492072	0.2161929	0.78494	2.199205	<.0001*
100% Activated C	8% Biochar	1.427139	0.2155255	0.72219	2.132089	<.0001*
4% Biochar	8% Biochar	1.342146	0.2159640	0.63576	2.048531	<.0001*
0% Biochar	2% Biochar	1.304361	0.2150825	0.60086	2.007862	<.0001*
50% Biochar	100% Graphite	1.297153	0.2164125	0.58930	2.005004	<.0001*
6% Biochar	100% Graphite	1.261032	0.2410590	0.47257	2.049498	<.0001*
10% Biochar	100% Biochar	1.189884	0.2395514	0.40635	1.973419	<.0001*
50% Graphite	2% Biochar	1.118381	0.2155255	0.41343	1.823331	<.0001*
100% Activated C	100% Biochar	1.103857	0.2150825	0.40036	1.807358	<.0001*
50% Activated C	2% Biochar	1.099853	0.2159749	0.39343	1.806273	<.0001*
0% Biochar	6% Biochar	1.040728	0.2408619	0.25291	1.828549	0.0010*
4% Biochar	100% Biochar	1.018864	0.2155219	0.31393	1.723803	0.0002*
50% Biochar	8% Biochar	1.015254	0.2166337	0.30668	1.723829	0.0002*
0% Biochar	50% Biochar	1.004607	0.2161929	0.29747	1.711740	0.0002*
2% Biochar	100% Graphite	0.997399	0.2153032	0.29318	1.701622	0.0002*
6% Biochar	8% Biochar	0.979133	0.2412576	0.19002	1.768249	0.0030*
50% Graphite	6% Biochar	0.854748	0.2412576	0.06563	1.643864	0.0206*
50% Activated C	6% Biochar	0.836220	0.2416592	0.04579	1.626649	0.0273*
50% Graphite	50% Biochar	0.818627	0.2166337	0.11005	1.527202	0.0088*
50% Activated C	50% Biochar	0.800099	0.2170808	0.09006	1.510137	0.0124*
10% Biochar	2% Biochar	0.797665	0.2393547	0.01477	1.580556	0.0413*
2% Biochar	8% Biochar	0.715500	0.2155255	0.01055	1.420450	0.0429*
100% Activated C	2% Biochar	0.711638	0.2148634	0.00885	1.414422	0.0440*
50% Biochar	100% Biochar	0.691972	0.2161929	-0.01516	1.399105	0.0618
0% Biochar	4% Biochar	0.677715	0.2155219	-0.02722	1.382653	0.0729
6% Biochar	100% Biochar	0.655852	0.2408619	-0.13197	1.443673	0.2153
4% Biochar	2% Biochar	0.626646	0.2153032	-0.07758	1.330869	0.1376
100% Biochar	100% Graphite	0.605181	0.2155219	-0.09976	1.310119	0.1770
0% Biochar	100% Activated C	0.592723	0.2150825	-0.11078	1.296224	0.1999
10% Biochar	6% Biochar	0.534032	0.2627635	-0.32543	1.393490	0.6711
0% Biochar	10% Biochar	0.506696	0.2395514	-0.27684	1.290231	0.6118
10% Biochar	50% Biochar	0.497911	0.2403530	-0.28825	1.284068	0.6433
50% Graphite	4% Biochar	0.491735	0.2159640	-0.21465	1.198120	0.4934
50% Activated C	4% Biochar	0.473207	0.2164125	-0.23464	1.181059	0.5596
100% Activated C	6% Biochar	0.448005	0.2406663	-0.33918	1.235187	0.7830
100% Activated C	50% Biochar	0.411884	0.2159749	-0.29454	1.118304	0.7550
50% Graphite	100% Activated C	0.406743	0.2155255	-0.29821	1.111693	0.7674
2% Biochar	100% Biochar	0.392219	0.2150825	-0.31128	1.095720	0.8052
50% Activated C	100% Activated C	0.388215	0.2159749	-0.31821	1.094635	0.8197
4% Biochar	6% Biochar	0.363013	0.2410590	-0.42545	1.151479	0.9393
4% Biochar	50% Biochar	0.326892	0.2164125	-0.38096	1.034743	0.9380
100% Biochar	8% Biochar	0.323282	0.2157440	-0.38238	1.028946	0.9413
50% Graphite	10% Biochar	0.320716	0.2399493	-0.46412	1.105552	0.9743
50% Activated C	10% Biochar	0.302188	0.2403530	-0.48397	1.088345	0.9840
50% Biochar	2% Biochar	0.299754	0.2159749	-0.40667	1.006174	0.9660
8% Biochar	100% Graphite	0.281899	0.2159640	-0.42449	0.988283	0.9786
6% Biochar	2% Biochar	0.263633	0.2406663	-0.52355	1.050815	0.9949
0% Biochar	50% Activated C	0.204508	0.2161929	-0.50263	0.911641	0.9986
0% Biochar	50% Graphite	0.185980	0.2157440	-0.51968	0.891644	0.9994
10% Biochar	4% Biochar	0.171019	0.2397496	-0.61316	0.955202	0.9999
10% Biochar	100% Activated C	0.086027	0.2393547	-0.69686	0.868918	1.0000
100% Activated C	4% Biochar	0.084992	0.2153032	-0.61923	0.789215	1.0000
50% Biochar	6% Biochar	0.036121	0.2416592	-0.75431	0.826550	1.0000
50% Graphite	50% Activated C	0.018528	0.2166337	-0.69005	0.727103	1.0000

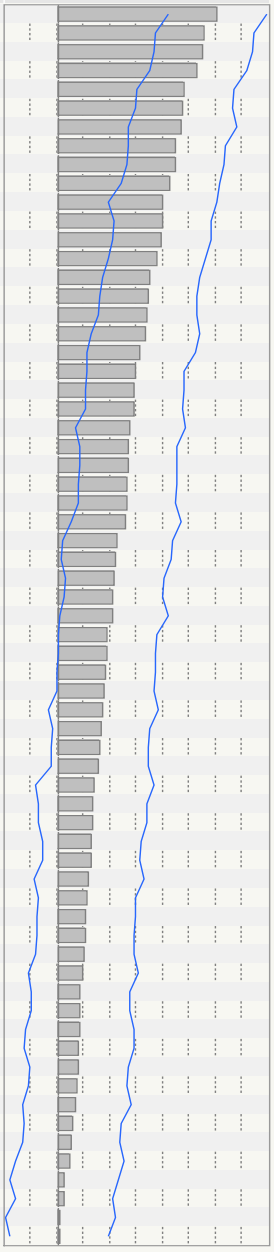

The correlation coefficients and corresponding p-values between attributes and C source and subgroups of C source are shown in Tables 12-15.

The Pearson correlation coefficients between biochar carbon content and attributes indicated that only area had a significant linear correlation with biochar at 0.1% level. Considering the integrated squared amplitude, the area was able to be detected by a subtler signal changes than the other three attributes. Since the correlation coefficient is negative 0.1047, the area will decrease when the biochar carbon content increases.

Table 12. Pearson correlation between attributes and biochar carbon content.

	Pearson correlation coefficient	P-value
Maximum amplitude	-0.0259	0.2722
Intensity	-0.0266	0.2607
Energy	-0.0146	0.5361
Area	-0.1047	8.81e-06***

Note: *, **, and *** denotes significance at 0.05, 0.01, and 0.001 level of probability, respectively.

Similar to biochar, the Pearson correlation coefficients between activated carbon carbon content and attributes indicated that only area had significant linear correlation with activated carbon at 0.1% level (Table 13). The correlation coefficient, being negative, (-0.1075), indicates that the area will decrease when the activated carbon content increases.

Table 13. Pearson correlation between attributes and activated carbon carbon content

	Pearson correlation coefficient	P-value
Maximum amplitude	0.0344	0.3522
Intensity	0.0713	0.0538
Energy	0.0596	0.107
Area	-0.1075	0.0036**

Note: *, **, and *** denotes significance at 0.05, 0.01, and 0.001 level of probability, respectively.

The Pearson correlation coefficients between graphite carbon content and attributes indicated all attributes had significant linear correlations with graphite at 0.1% level (Table 14). The correlation coefficients between the three attributes (maximum amplitude, intensity, and energy) and graphite carbon content were all positive, indicating the value of these three attributes increases when graphite carbon content increases. As for area, the correlation coefficient with graphite carbon content was negative, (-0.1075); therefore, so the area decreases when activated carbon content increases. The negative relationship could be caused by the method of calculating the area. The area was estimated from a different strength of the signal amplitude. First, the amplitude was squared and then integrated along the x axis. Therefore, area contained more information than the other three attributes, Moreover, the area would carry more unnecessary information than the others. Morris and Glisic (2017) conducted a similar analysis using concrete and bricks. The correlation coefficient between the mass of the samples and the area was the highest among the other attributes, similar to the results in this research.

Table 14.Pearson correlation between attributes and graphite carbon content.

	Pearson correlation coefficient	P-value
Maximum amplitude	0.2650	3.13e-13***
Intensity	0.2528	3.87e-12***
Energy	0.3131	<2.20e-16***
Area	-0.3735	<2.20e-16***

Note: *, **, and *** denotes significance at 0.05, 0.01, and 0.001 level of probability, respectively.

The criteria for grouping biochar and activated carbon was based on the significance of the Tukey's HSD test between each treatment. For each attribute, the biochar treatment was selected when it was significantly different from 50% and 100% activated carbon. A reason why some biochar treatment attributes were not significantly different from another treatment is that the carbon content of the biochar used was very low. GPR was not be able to detect the difference among signals. Thus, the attributes were reflecting the signals from the silicon sample bag or the sand. The Pearson correlation coefficients between the sub-group (activated carbon and biochar carbon content) and the four attributes revealed that all the attributes have a significant linear correlation at 0.1% level (Table 15). The correlation coefficient between maximum amplitude and graphite carbon content was -0.2178. This shows the maximum amplitude decreases when the graphite carbon content increases. The correlation coefficient between intensity and graphite carbon content was -0.1913, indicating the intensity decreases as the graphite carbon content increases. The correlation coefficient between energy and graphite carbon content was -0.1937, showing that energy decreases when the graphite carbon content increases. As for area, the correlation coefficient with graphite carbon content was 0.1029, indicating the area increases when activated carbon content increases. Note the correlation coefficients changed between single (biochar alone, activated carbon alone) and the combined as a sub-group. The values strengthen the negative correlation for the three attributes but reverses the relationship for area. The reversal might come from error during data collection or the fact that subgroup treatments based on Tukey's HSD test would bring the most potentially different

combination which resulted in the most significant and precise correlation. Moreover, since area was transformed the most from the original data, it carries some unwanted data which could bring more information, thereby affecting the results. But for biochar and activated carbon, area was the only attribute that had significant correlation, indicating that area could be a useful predictor as long as possibly redundant data is removed. Among all the correlation coefficients, the coefficient between graphite carbon content and area was the highest. This indicates the area of GPR data responded stronger to pure sand than graphite. Moreover, graphite was easier for GPR to identify than biochar and activated carbon.

Table 15. Pearson correlation between attributes and biochar and activated subgroup carbon content.

	Pearson correlation coefficient	P-value
Maximum amplitude	-0.2178	2.79e-16***
Intensity	-0.1913	7.69e-13***
Energy	-0.1937	1.11e-09***
Area	0.1029	3.22e-05***

Note: *, **, and *** denotes significance at 0.05, 0.01, and 0.001 level of probability, respectively.

Naïve Bayes Predictive Model

To further assess the ability of GPR to identify different carbon contents and carbon structures, two naïve Bayes predictive models were constructed. Naïve bayes modeling uses Bayes' theorem with independence assumption between features to construct a classifier. The predictive model can develop a baseline for different percentages of carbon and different structures of carbon. With additional data collected, its accuracy is expected to be higher.

To classify the different carbon contents, the classifications of the model were: 2%, 4%, 6%, 8%, 10%, 50%, and 100% biochar, 50% and 100% activated carbon, and 50% and 100% graphite. The parameters used to build the model were maximum amplitude, intensity, energy, and area. To validate the accuracy of the model, the data was split into 75/25 ratio as training and validation set. This ratio was used because the data set sample size was not large enough to support a 50/50 ratio for 12 treatments as classifiers.

The AUC-ROC curve was used to estimate the ability of the model to distinguish different classes. AUC represents Area Under the Curve and ROC represents Receiver Operating Characteristics. With higher AUC, the better the model predicted classes. The accuracy remained above 50 to 60 percent for each treatment (Table 15). The highest AUC of validation from the carbon content predictive model was 70% (0.6944), which predicted 8% of the biochar.

Table 16. Naïve Bayes predictive model for carbon content.

Carbon percentage	AUC of Training	AUC of Validation
0% biochar	0.6548	0.6268
2% biochar	0.5672	0.5677
4% biochar	0.5322	0.5649
6% biochar	0.5745	0.5791
8% biochar	0.6565	0.6944
10% biochar	0.6281	0.6572
50% biochar	0.5364	0.6341
100% biochar	0.5737	0.6370
50% activated carbon	0.6225	0.6716
100% activated carbon	0.5845	0.5657
50% graphite	0.5762	0.5289
100% graphite	0.6924	0.6162

To classify the different carbon structures, the parameters used to construct the model included all the four attributes, and the classification was sand, biochar, graphite, and activated carbon. The data also was split with 75/25 ratio as training and validation set similar as above for carbon content. Except for graphite, AUC for biochar, activated carbon, and sand are all more than 0.6000 (Table 16). This indicates that within each group with the carbon content being different the attributes are still capable of identifying different carbon structures.

Table 17. Naïve Bayes predictive model for carbon structure and sand.

Structure	AUC of Training	AUC of Validation
Biochar	0.5980	0.6230
Activated carbon	0.5716	0.6014
Graphite	0.5714	0.4933
Sand	0.6501	0.6240

CHAPTER V

CONCLUSION

There were four objectives of this research: (1) Use ground penetrating radar to detect underground biochar amended soil carbon content; (2) Compare the performance of GPR across materials with different structures of carbon; (3) Compare the performance of GPR across different soil moisture levels; (4) Develop novel GPR analysis methods to quantify carbon. For the first objective, the naïve Bayes predictive model for carbon content demonstrated that at approximately 0.6944 accuracy, the GPR was able to detect biochar amended soil. The second objective was well supported by the naïve Bayes predictive model for carbon structure, with only the graphite prediction accuracy was as low as 0.4933, the other two carbon structures maintained an AUC over 0.6000. The Spearman rank correlation tests across three moisture levels for all attributes were significant, indicating the ability of detecting soil moisture level of the GPR. Since all the coefficients were positive, indicating that higher moisture level was easier to be detected. Therefore, they well support the third objective. Moreover, the highest correlation coefficient was 0.1990 between area and moisture level. All correlation coefficients were positive, so with higher moisture level the attribute was higher as well. The last objective was backed by the Pearson correlation coefficients between attributes and carbon content. Unlike the correlation with moisture level, the correlation coefficients between attributes and carbon content were mostly negative, showing that quantification of carbon content is difficult at varying water content using GPR. All

correlation coefficients between graphite carbon content and attributes were significant, and for activated carbon and biochar carbon content, their correlations with area were significant. Grouping activated carbon and biochar together, the correlation coefficients were significant with attributes. This was observed because the structure difference, and random interfere during data collection. A replication of this research for the next year can further validate the inconsistency of the correlation coefficient. As for the predictive model, the results indicate that more sampling data is needed. During this study, 3868 samples were collected and after excluding two boarder channels, the number of samples were reduced to 2767, and each classification were assigned to around 240 samples. Although the data set for each classification was not large enough, the accuracy obtained were still remained about 50%, indicating the great potential of the naïve Bayes predictive model in classifying different carbon content. The further research could focus on collecting more data and applying more appropriate attributes and perfecting naïve Bayes predictive model to increase the prediction accuracy.

REFERENCES

Amundson, R., Berhe, A.A., Hopmans, J.W., Olson, C., Sztein, A.E., and Sparks, D.L.: Soil and human security in the 21st century, Science, 348, 1261071, doi: 10.1126/science.1261071, 2015.

Anbazhagan, P., Dixit, P.N. and Bharatha, T.P.: Identification of type and degree of railway ballast fouling using ground coupled GPR antennas. J. Appl. Geophys., 126, 183-190, doi: 10.1016/j.jappgeo.2016.01.018, 2016.

Batjes, N.H.: Mitigation of atmospheric CO_2 concentrations by increased carbon sequestration in the soil, Biol. Fert. Soils, 27, 230-235, doi: 10.1007/s003740050425, 1998.

Benedetto, F., and Tosti, F.: GPR spectral analysis for clay content evaluation by the frequency shift method, J. Appl. Geophy., 97, 89-96, doi: 10.1016/j.jappgeo.2013.03.012, 2013.

Boden, T.A., Marland, G., and Andres, R.J.: Global, Regional, and National Fossil-Fuel CO_2 Emissions, United States, https://www.osti.gov/servlets/purl/1389326, 2011.

Bridgwater, A.V., Meier, D., and Radlein, D.: An overview of fast pyrolysis of biomass, Org. Geochem., 30, 1479-1493, doi: 10.1016/S0146-6380(99)00120-5, 1999.

Brovelli, A., Cassiani, G.: Linking soil properties to permittivity data: Beyond the refractive index model, in: CMWR XVI Computational Methods in Water Resources, Copenhagen, Denmark, 19-22 June, 2006.

Brown, R.C., and Brown, T. R.: Biorenewable resources: engineering new products from agriculture, 2nd edition, John Wiley & Sons, Hoboken, New Jersey, United States, 2013.

Bruun, E.W., Ambus, P., Egsgaard, H., and Hauggaard-Nielsen, H.: Effects of slow and fast pyrolysis biochar on soil C and N turnover dynamics, Soil Biology and Biochemistry, 46, 73-79, doi: 10.1016/j.soilbio.2011.11.019, 2012.

Butnor, J.R., Doolittle, J.A., Kress, L., Cohen, S., and Johnsen, K.H.: Use of ground pene- trating radar to study tree roots in the southeastern United States, Tree Physiol., 21, 1269–1278, doi: 10.1093/treephys/21.17.1269, 2001.

Cassidy, N. J.: Ground Penetrating Radar Data Processing, Modelling and Analysis, in: Ground Penetrating radar: Theory and Application, edited by: Jol, H.M, Elsevier Science, Amsterdam, The Netherlands.

Cassidy, N.J.: Electrical and magnetic properties of rocks, soilsand fluids, in: Ground Penetrating Radar Theory and Applications, edited by: Jol, H. M., Elsevier, Amsterdam, Netherlands, 41-67, 2008.

Clough, T.J., Bertram, J.E., Ray, J.L., Condron, L.M., O'Callaghan, M., Sherlock, R.R., and Wells, N.S.: Unweathered wood biochar impact on nitrous oxide emissions from a bovine-urine-amended pasture soil, Soil Sci. Soc. Am. J., 74, 852-860, doi: 10.2136/sssaj2009.0185, 2010.

Comas, X., Terry, N., Warren, M., Kolka, R., Kristiyono, A., Sudiana, N., and Darusman, T: Imaging tropical peatlands in Indonesia using ground-penetrating radar (GPR) and electrical resistivity imaging (ERI): implications for carbon stock estimates

and peat soil characterization, Biogeosciences, 12, 2995-3007, doi: 10.5194/bg-12-2995-2015, 2015.

Conyers, L. B., Ground-Penetrating Radar for Archaeology, 2nd edition. Oxford: AltaMira, 2004.

Crowther, T.W., Todd-Brown, K.E., Rowe, C.W., Wieder, W.R., Carey, J.C., Machmuller, M.B., Snoek, B.L., Fang, S., Zhou, G., Allison, S.D. and Blair, J.M.: Quantifying global soil carbon losses in response to warming, Nature, 540, 104, doi: 10.1038/nature20150, 2016.

De Deyn, G.B., Cornelissen, J.H., and Bardgett, R.D.: Plant functional traits and soil carbon sequestration in contrasting biomes, Ecol. Lett., 11, 516-531, doi: 10.1111/j.1461-0248.2008.01164.x, 2008.

Dogan, M., and Turhan-Sayan, G.: Preprocessing of A-scan GPR data based on energy features, Detection and Sensing of Mines, Explosive Objects, and Obscured Targets, 9823, 98231, 2016.

El-Mahallawy, M.S. and Hashim, M.: Material classification of underground utilities from GPR images using DCT-based SVM approach. IEEE Geoscience and Remote Sensing Letters, 10, 1542-1546, doi: 10.1016/j.ndteint.2013.11.006, 2013.

Feng, K., Zhao, Y., Zhang, Z., and Ge, S.: Stratigraphic absorption compensation of GPR signal based on improved S-transform, in: 2015 8th International Workshop on Advanced Ground Penetrating Radar (IWAGPR), Florence, Italy, 7-10 July 2015, 1-4, 2015.

Fowles, M.: Black carbon sequestration as an alternative to bioenergy, Biomass and Bioenergy, 31, 426-432, doi: 10.1016/j.biombioe.2007.01.012, 2007.

Gader, P.D., Mystkowski, M., Zhao, Y.: Landmine detection with ground penetrating radar using hidden Markov models, IEEE. Trans. Geosci. Remote. Sens., 39, 1231-1244, doi: 10.1109/36.927446, 2001.

Glaser, B., Haumaier, L., Guggenberger, G., and Zech, W.: The'Terra Preta'phenomenon: a model for sustainable agriculture in the humid tropics, Naturwissenschaften, 88, 37-41, doi: 10.1007/s001140000193, 2001.

Greenhouse Gases and Carbon Sequestration in Agriculture and Forestry, USDA Baltimore, Maryland, United States, 21-24 March 2005.

Hammes, K., Schmidt, M.W., Smernik, R.J., Currie, L.A., Ball, W.P., Nguyen, T.H., Louchouarn, P., Houel, S., Gustafsson, Ö., Elmquist, M. and Cornelissen, G.: Comparison of quantification methods to measure fire-derived (black/elemental) carbon in soils and sediments using reference materials from soil, water, sediment and the atmosphere, Global Biogeochem. Cycles, 21, GB3016, doi: 10.1029/2006GB002914, 2007.

Heil, C.E., Walnut, D.F.: Continuous and discrete wavelet transforms, SIAM review, 31, 628-666, 1989.

Herzog, H.J.: Peer reviewed: what future for carbon capture and sequestration, *Environ. Sci. Technol.*, 35, 148A–153A, doi: 10.1021/es012307j, 2001.

Howden, S.M., Soussana, J.F., Tubiello, F.N., Chhetri, N., Dunlop, M. and Meinke, H.: Adapting agriculture to climate change. Proceedings of the national academy of sciences, 104, 19691-19696, doi: 10.1073/pnas.0701890104, 2007.

Iryanti, M., Nugraha, H.D., Setiawan, T., and Bijaksana, S.: Mapping peat morphology in sag pond with ground penetrating radar, AIP Conference Proceedings, 1861, 265-268, doi: 10.1063/1.4820336, 2013.

Javadi, M., Ghasemzadeh, H.: Wavelet analysis for ground penetrating radar applications: a case study, Journal of Geophysics and Engineering, 14, 1189-1202, 2017

Jol, H.M., and Smith, D.G.: Ground penetrating radar surveys of peatlands for oilfield pipelines in Canada, J. Appl. Geophys., 34, 109-123, doi: 10.1016/0926-9851(95)00018-6, 1995.

Kowalsky, M.B., Finsterle, S., Peterson, J., Hubbard, S., Rubin, Y., Majer, E., Ward, A., and Gee, G.: Estimation of field-scale soil hydraulic and dielectric parameters through joint inversion of GPR and hydrological data, Water Resources Research, 41, 11, 2005.

Laird, D.A.: The charcoal vision: a win–win–win scenario for simultaneously producing bioenergy, permanently sequestering carbon, while improving soil and water quality, Agron. J., 100, 178-181, doi: 10.2134/agronj2007.0161, 2008.

Lal, R., Delgado, J.A., Groffman, P.M., Millar, N., Dell, C., and Rotz, A.: Management to mitigate and adapt to climate change, J. Soil Water Conserv., 66, 276-285, doi: 10.2489/jswc.66.4.276, 2011.

Lal, R.: World cropland soils as a source or sink for atmospheric carbon, Adv. Agron., 71, 145-191, doi: 10.1016/S0065-2113(01)71014-0, 2001.

Le Gall, A., Ciarletti, V., Berthelier, J.J., Reineix, A., Guiffaut, C., Ney, R., Dolon, F., and Bonaime, S.: An imaging HF GPR using stationary antennas: experimental validation over the Antarctic ice sheet. IEEE. Trans. Geosci. Remote. Sens., 46, 3975–3986, doi: 10.1109/TGRS.2008.2000718, 2008.

Lee, D.T. and Yamamoto, A.: Wavelet analysis: theory and applications. Hewlett Packard Journal, 45, 44, 1994.

Lee, G., Wasilewski, F., Gommers, R., Wohlfahrt, K., O'Leary, A., and Nahrstaedt, H.: PyWavelets - Wavelet Transforms in Python,
2006, https://github.com/PyWavelets/pywt.

Lehmann, J., Gaunt, J., and Rondon, M.: Bio-char sequestration in terrestrial ecosystems–a review, Mitig. Adapt. Strat. Gl., 11, 403-427, doi: 10.1007/s11027-005-9006-5, 2006.

Lehmann, J.: A handful of carbon, Nature, 447, 143-144, 2007.

Lenton, T.M., and Vaughan, N.E.: The radiative forcing potential of different climate geoengineering options, Atmos. Chem. Phys., 9, 5539-5561, doi: 10.5194/acp-9-5539-2009, 2009.

Li, C., and Mu, M.: Relationship between East Asian winter monsoon, warm pool situation and ENSO cycle, Chinese. Sci. Bull., 45, 1448, doi: 10.1007/BF02898885, 2000.

Li, L., Xia, Y.H., Liu, S.J., Zhang, W., Chen, X.B., Zheng, H., Qiu, H.S., He, X.Y. and Su, Y.R.: Modified method for estimating organic carbon density in discontinuous Karst

soil using ground-penetrating radar and geostatistics, J. Mt. Sci., 12, 1229-1240, doi: 10.1007/s11629-015-3431-z, 2015.

Liu, X., Dong, X. and Leskovar, D.I., 2016. Ground penetrating radar for underground sensing in agriculture: a review. International Agrophysics, 30, 533-543, doi: 10.1515/intag-2016-0010, 2016.

Loisel, J., Yu, Z., Parsekian, A., Nolan, J., and Slater, L.: Quantifying landscape morphology influence on peatland lateral expansion using ground-penetrating radar (GPR) and peat core analysis, J. Geophys. Res-Biogeo., 118, 373-384, doi: 10.1002/jgrg.20029, 2013.

McCallum, A. and Nigam, K.: A comparison of event models for naive bayes text classification, in: AAAI-98 workshop on learning for text categorization, Madison, Wisconsin, USA, 26-27 July, 52, 1998, 41-48, 1998

McClellan, M., Comas, X., Benscoter, B., Hinkle, R., & Sumner, D.: Estimating belowground carbon stocks in isolated wetlands of the Northern Everglades Watershed, central Florida, using ground penetrating radar and aerial imagery, J. Geophys. Res-Biogeo., 12, 2804-2816, doi 10.1002/2016JG003573, 2017.

Mohan, D., Pittman, C.U., and Steele, P.H.: Pyrolysis of wood/biomass for bio-oil: a critical review, Energ. Fuel., 20, 848-889, doi: 10.1021/ef0502397, 2006

Montanarella, L., Pennock, D.J., McKenzie, N., Badraoui, M., Chude, V., Baptista, I., Mamo, T., Yemefack, M., Singh Aulakh, M., Yagi, K. and Young Hong, S.: World's soils are under threat., Soil, 2, 79-82, doi: 10.5194/soil-2-79-2016, 2016.

Morris, I., Glisic, B.: Archaeological Ground Penetrating Radar Surveys Under Variable Soil Moisture: Visual and Numerical Results, in: 2017 9th International Workshop on Advanced Ground Penetrating Radar, Edinburgh, UK, 28-30 June, 2017, 1-5, doi: 10.1109/IWAGPR.2017.7996070, 2017.

Ng, W., Chan, T.C.T., So, H.C., and Ho, K.C.: Particle filtering based approach for landmine detection using ground penetrating radar, IEEE. Trans. Geosci. Remote. Sens., 46, 3739-3755, doi: 10.1109/TGRS.2008.2002028, 2008.

Nicolotti, G., Socco, L.V., Martinis, R., Godio, A., and Sambuelli, L.: Application and comparison of three tomographic techniques for detection of decay in trees. Journal of Arboriculture, 29, 66-78, 2003.

Olhoeft, G.R.: Electrical properties from 10^{-3} Hz to 10^{+9} Hz - physics and chemistry. American Institute of Physics Conference Proceeding 1987, Anaheim, California, USA, 281-298, 1987.

Onay, O., and Kockar, O.M.: Slow, fast and flash pyrolysis of rapeseed, Renew. Energy., 28, 2417-2433, doi: 10.1016/S0960-1481(03)00137-X, 2003.

Pang, B., Lee, L., and Vaithyanathan, S.: Thumbs up?: sentiment classification using machine learning techniques, in: Proceedings of the ACL-02 conference on Empirical methods in natural language processing, Stroudsburg, Pennsylvania, 2002, 10, 79-86, Association for Computational Linguistics, 2002.

Parsekian, A.D., Slater, L., Ntarlagiannis, D., Nolan, J., Sebesteyen, S.D., Kolka, R.K., and Hanson, P. J.: Uncertainty in peat volume and soil carbon estimated using ground-

penetrating radar and probing, Soil Sci. Soc. Am. J., 76, 1911-1918, doi: 10.2136/sssaj2012.0040, 2012.

Piao, S., Ciais, P., Huang, Y., Shen, Z., Peng, S., Li, J., Zhou, L., Liu, H., Ma, Y., Ding, Y. and Friedlingstein, P.: The impacts of climate change on water resources and agriculture in China. Nature, 467, 43, 2010.

Plass, G.N.: The carbon dioxide theory of climatic change, Tellus, 8. 140-154, 1955.

Post, W.M., and Kwon, K.C.: Soil carbon sequestration and land-use change: processes and potential. Glob. Change Bio., 6, 317-327, doi: 10.1046/j.1365-2486.2000.00308.x, 2000.

Rennie, J.D., Shih, L., Teevan, J. and Karger, D.R.: Tackling the poor assumptions of naive bayes text classifiers, in: Proceedings of the 20th international conference on machine learning, Washington, DC, USA, 21-24, August, 2003, 616-623, 2003.

Rish, I.: An empirical study of the naive Bayes classifier, in: IJCAI 2001 workshop on empirical methods in artificial intelligence, Seattle, USA, 4-6 August, 2001, 3, 41-46, 2001

Rondon, M., Ramirez, J.A., and Lehmann, J.: Charcoal additions reduce net emissions of greenhouse gases to the atmosphere, in: In Proceedings of the 3rd USDA Symposium on Scharpenseel, H.W., and Becker-Heidmann, P.: Sustainable Land Use in the Light of Resilience/Elasticity to Soil Organic Matter Functions, in: Soil Resilience and Sustainable Land Use, edited by: Greenland, D.J., and Szabolcs, I., CAB International, Wallingford, Oxon, UK, 249-262, 1994.

Schlesinger, W.: Biogeochemistry, Treatise on Geochemistry, 1st edition, Vol 8, Elsevier, New York, United States, 2005.

Schumacher, B.A.: Methods for the determination of total organic carbon (TOC) in soils and sediments, U.S. Environmental Protection Agency, Washington, DC, United States, 2002.

Shackley, S., Hammond, J., Gaunt, J., and Ibarrola, R.: The feasibility and costs of biochar deployment in the UK, Carbon Manag., 2, 335-356, doi: 10.4155/cmt.11.22, 2011.

Singh, B.P., Hatton, B. J., Singh, B., Cowie, A. L., and Kathuria, A.: Influence of biochars on nitrous oxide emission and nitrogen leaching from two contrasting soils, J. Environ. Qual., 39, 1224-1235, doi: 10.2134/jeq2009.0138, 2010.

Solla, M., Lagüela, S., González-Jorge, H., and Arias, P.: Approach to identify cracking in asphalt pavement using GPR and infrared thermographic methods: Preliminary findings. Ndt & E International, 62, 55-65, doi: 10.1109/LGRS.2013.2261796, 2014.

Sombroek, W.G., Nachtergaele, F.O., and Hebel, A.: Amounts, dynamics and sequestering of carbon in tropical and subtropical soils, Ambio, 22, 417-426, 1993.

Stokes, A., Fourcaud, T., Hruska, J., Cermak, J., Nadyezdhina, N., Nadyezhdin, V., and Praus, L.: An evaluation of different methods to investigate root system architecture of urban trees in situ: I. Ground-penetrating radar, Journal of Arboriculture, 28, 2-10, 2002.

Topp, G.C., Davis, J.L., and Annan, A.P.: Electromagnetic determination of soil water content: Measurements in coaxial transmission lines, Water Resour. Res., 16, 574-582, doi: 10.1029/WR016i003p00574, 1980.

Van Dam, R.: Calibrations Functions for estimating soil moisture from GPR dielectric constant measurements, Comm. In Soil Sci. and Plant Analysis, 45, 392-413, doi: 10.1080/00103624.2013.854805, 2014.

Van Zwieten, L., Kimber, S., Morris, S., Downie, A., Berger, E., Rust, J., and Scheer, C.: Influence of biochars on flux of N_2O and CO_2 from Ferrosol, Soil Res., 48, 555-568, 10.1071/SR10004, 2010.

West, T. O., and Post, W.M.: Soil organic carbon sequestration rates by tillage and crop rotation, Soil Sci. Soc. Am. J., 66, 1930-1946, doi: 10.2136/sssaj2002.1930, 2002.

Woolf, D., Amonette, J.E., Street-Perrott, F.A., Lehmann, J., and Joseph, S.: Sustainable biochar to mitigate global climate change, Nat. Commun., 1, 56, doi: 10.1038/ncomms1053, 2010.

Yu, O.Y., Harper, M., Hoepfl, M., and Domermuth, D.: Characterization of biochar and its effects on the water holding capacity of loamy sand soil: Comparison of hemlock biochar and switchblade grass biochar characteristics, Environ. Prog. Sustain. Energy, 36, 1474-1479, doi: 10.1002/ep.12592, 2017.

Zhang, A., Bian, R., Pan, G., Cui, L., Hussain, Q., Li, L., Zheng, J., Zheng, J., Zhang, X., Han, X. and Yu, X.: Effects of biochar amendment on soil quality, crop yield and greenhouse gas emission in a Chinese rice paddy: a field study of 2 consecutive rice growing cycles, Field Crop Res., 127, 153-160, doi: 10.1016/j.fcr.2011.11.020, 2012.

APPENDIX A

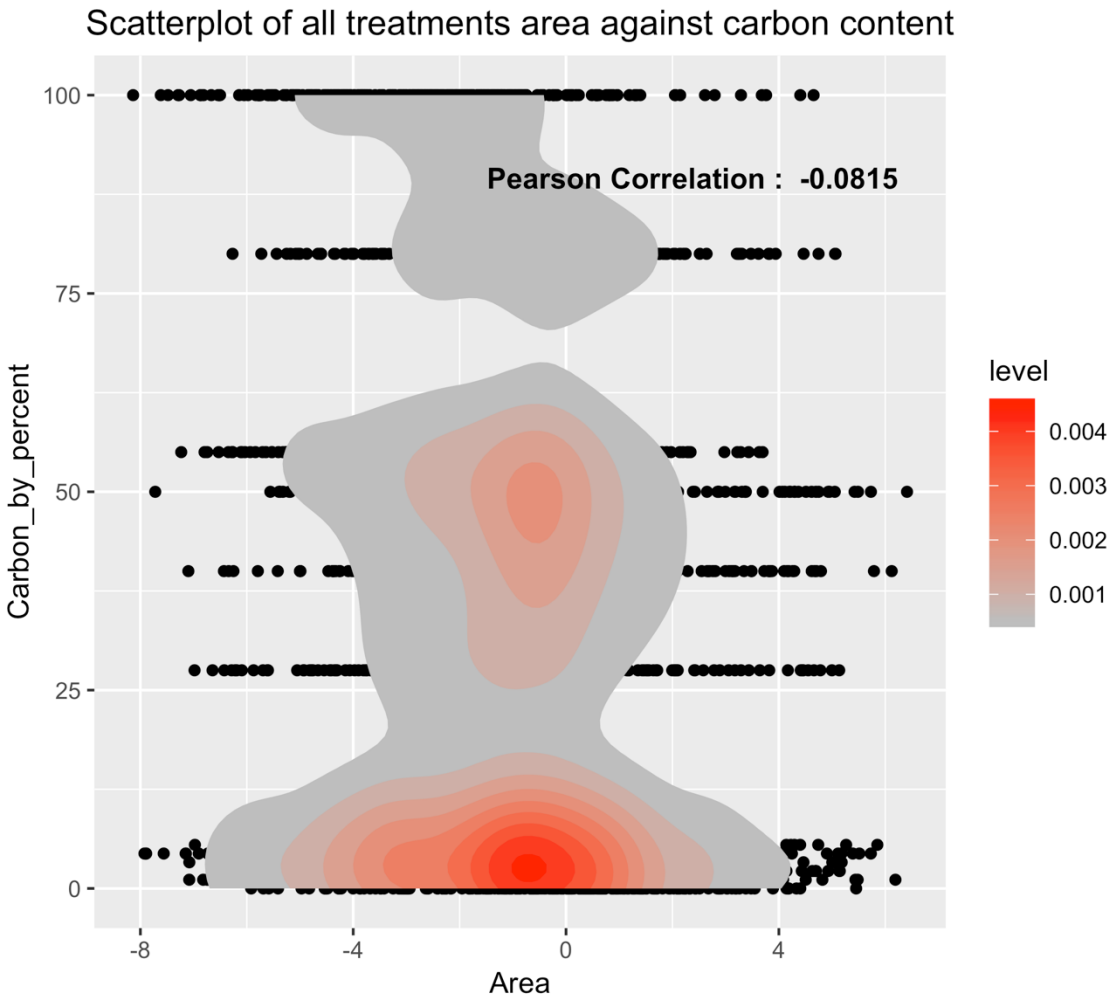

Figure 15. Scatterplot of all treatments area against carbon content with correlation coefficient.

The color of red represented how the points dense together, and the Pearson correlation coefficient between all treatments area and carbon content was -0.0815.

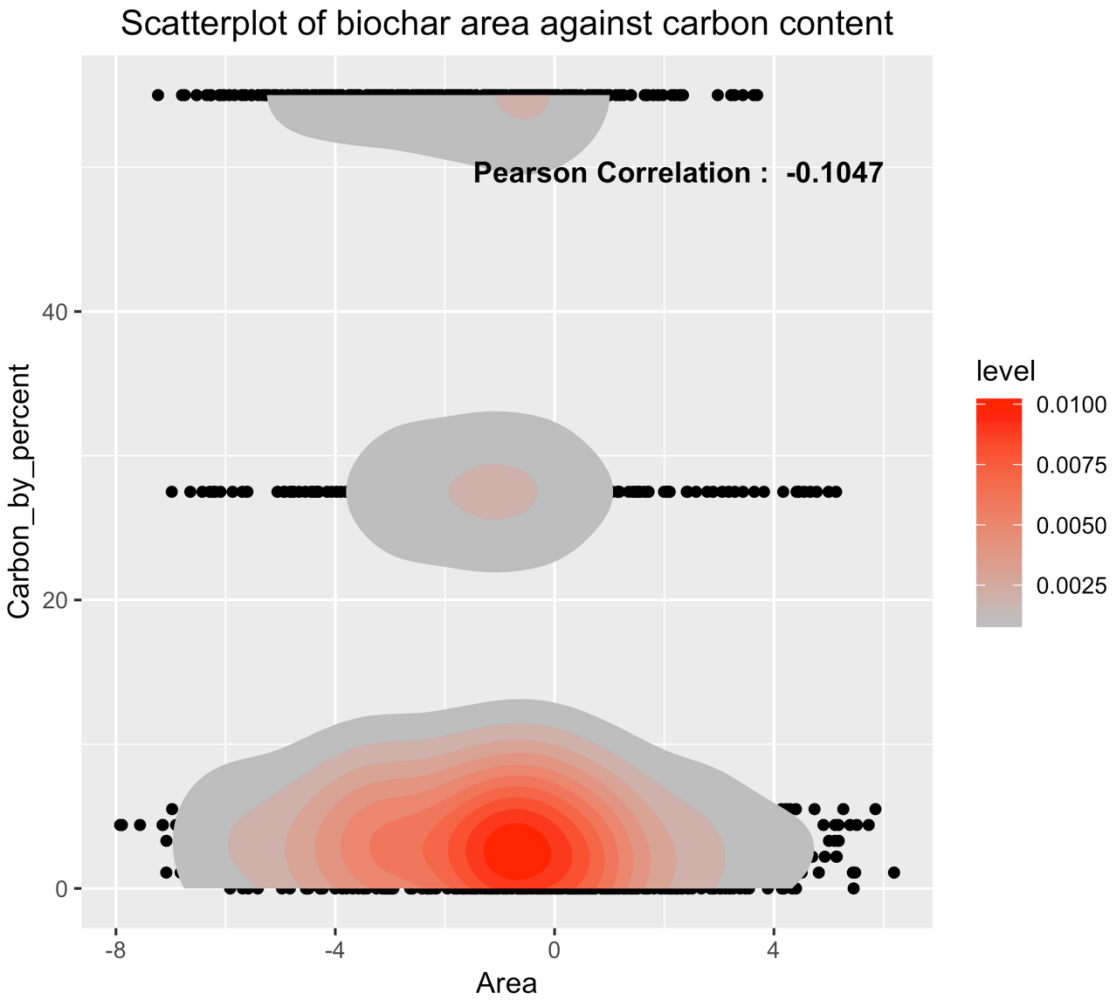

Figure 16. Scatterplot of biochar area against carbon content with correlation coefficient.

The color of red represented how the points dense together, and the Pearson correlation coefficient between biochar area and carbon content was -0.1047.

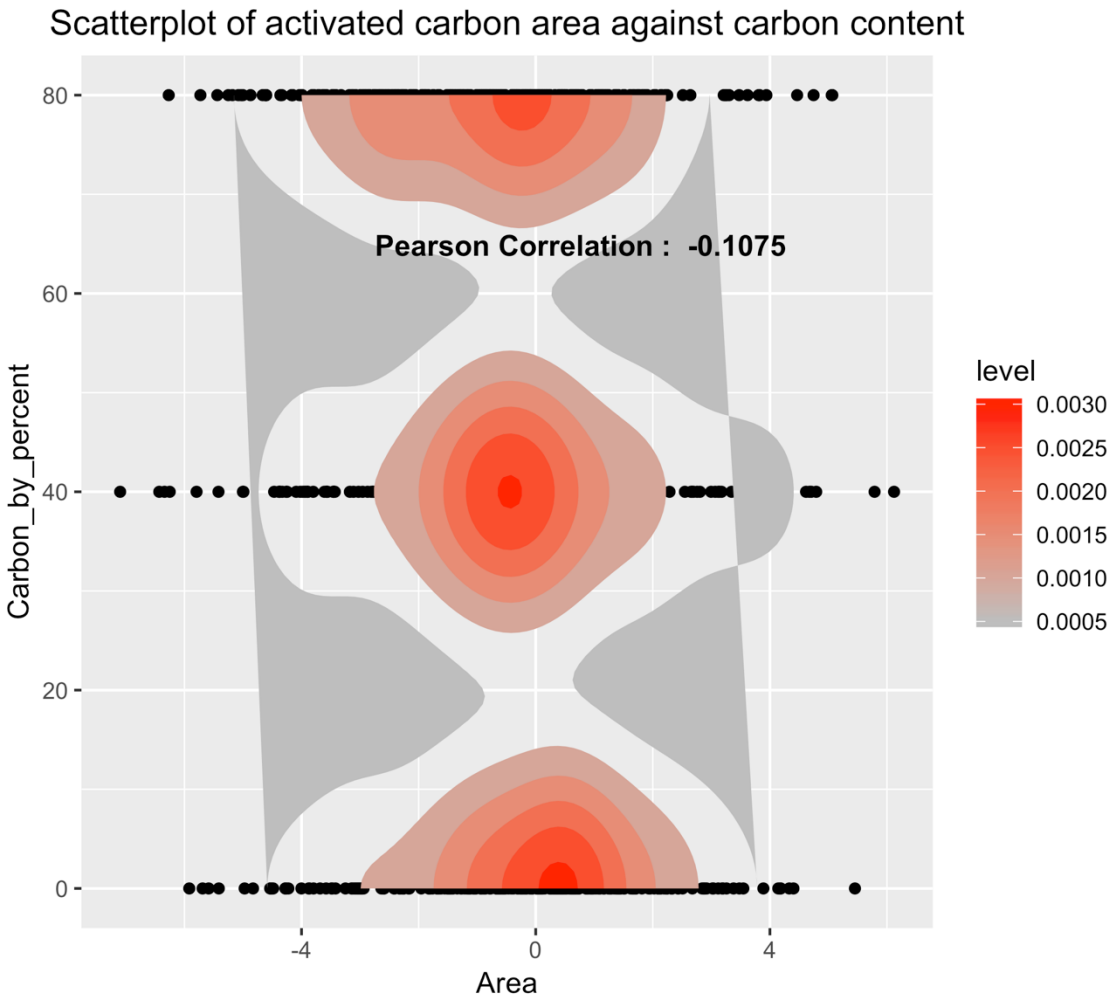

Figure 17. Scatterplot of activated carbon area against carbon content with correlation coefficient.

The color of red represented how the points dense together, and the Pearson correlation coefficient between activated carbon area and carbon content was -0.1075.

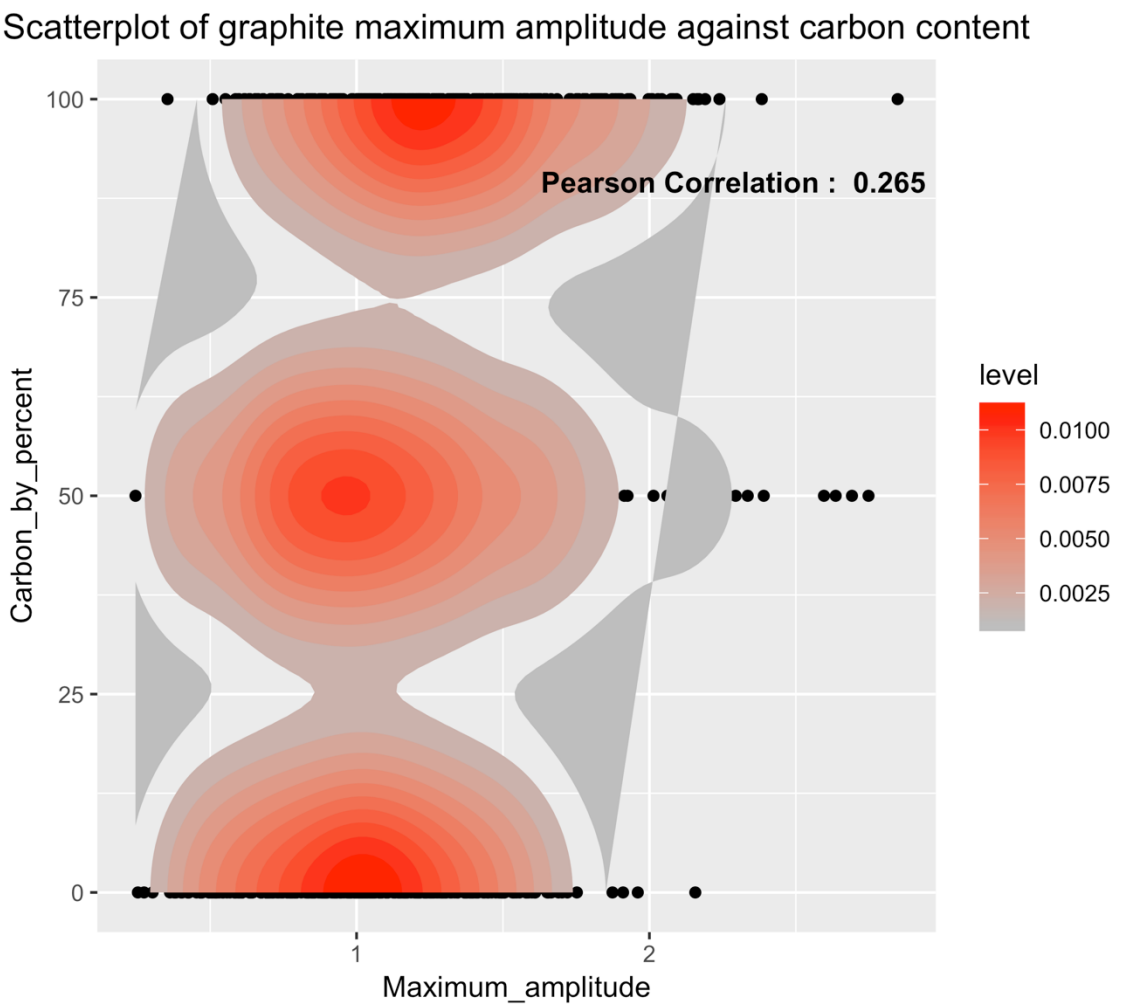

Figure 18. Scatterplot of graphite maximum amplitude against carbon content with correlation coefficient.

The color of red represented how the points dense together, and the Pearson correlation coefficient between graphite maximum amplitude and carbon content was 0.2650.

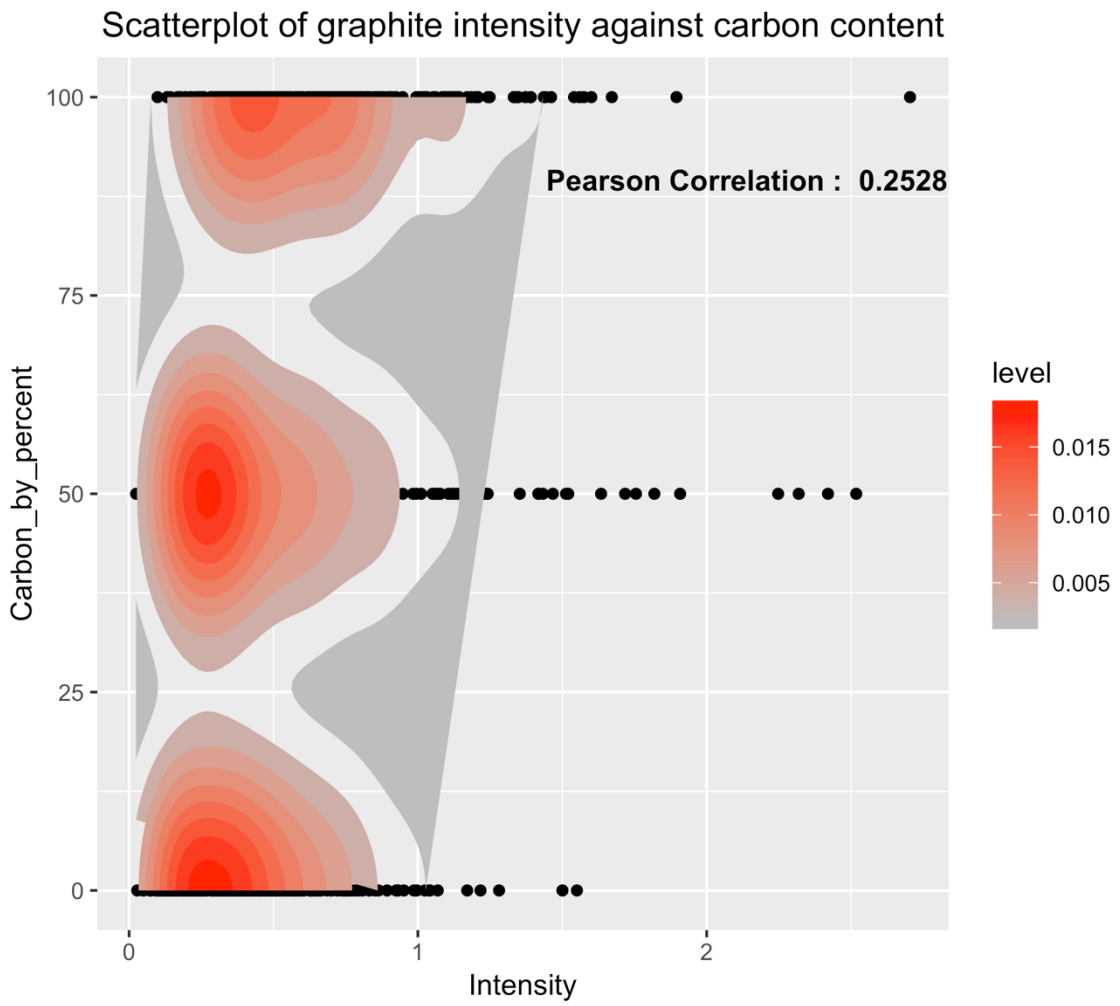

Figure 19. Scatterplot of graphite intensity against carbon content with correlation coefficient.

The color of red represented how the points dense together, and the Pearson correlation coefficient between graphite intensity and carbon content was 0.2528.

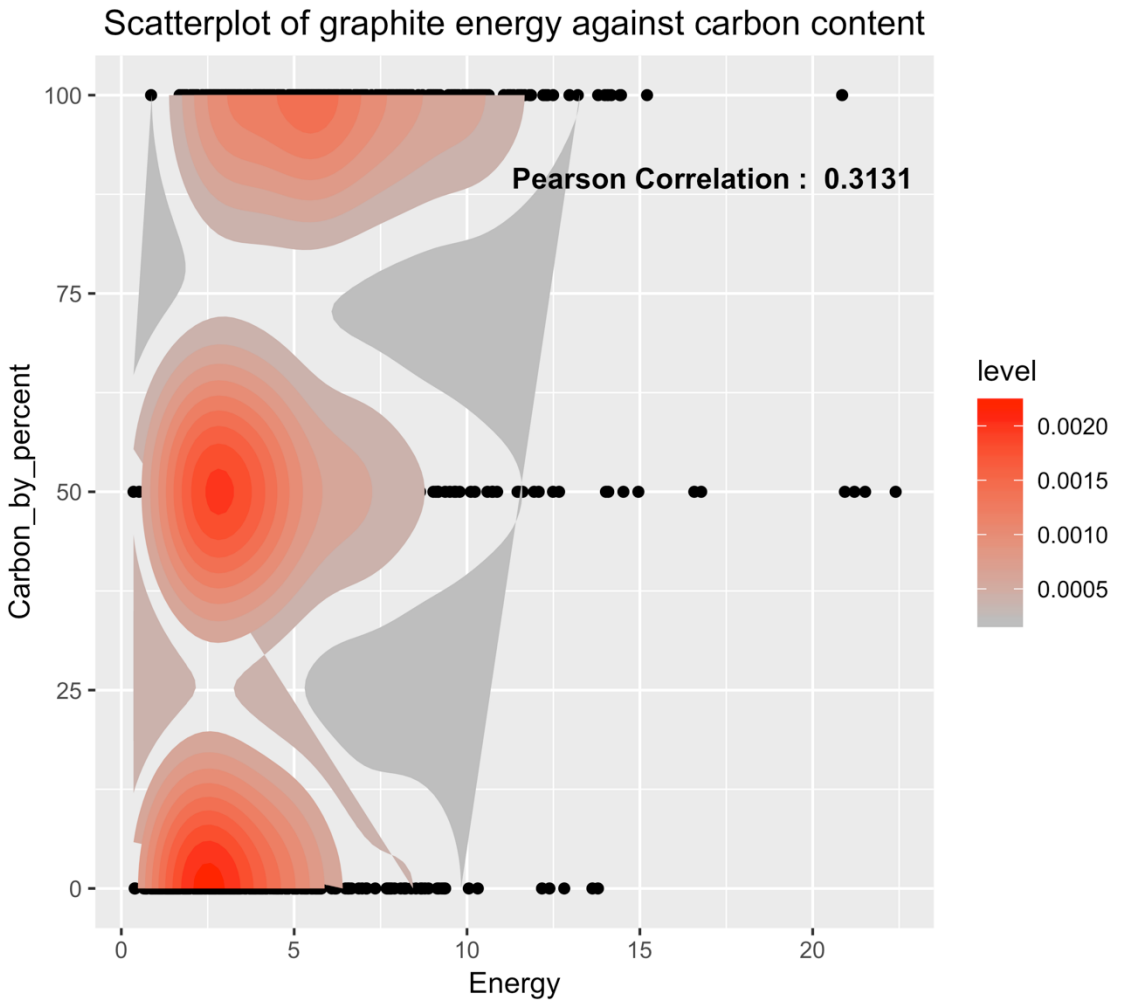

Figure 20. Scatterplot of graphite intensity against carbon content with correlation coefficient.

The color of red represented how the points dense together, and the Pearson correlation coefficient between graphite energy and carbon content was 0.3131.

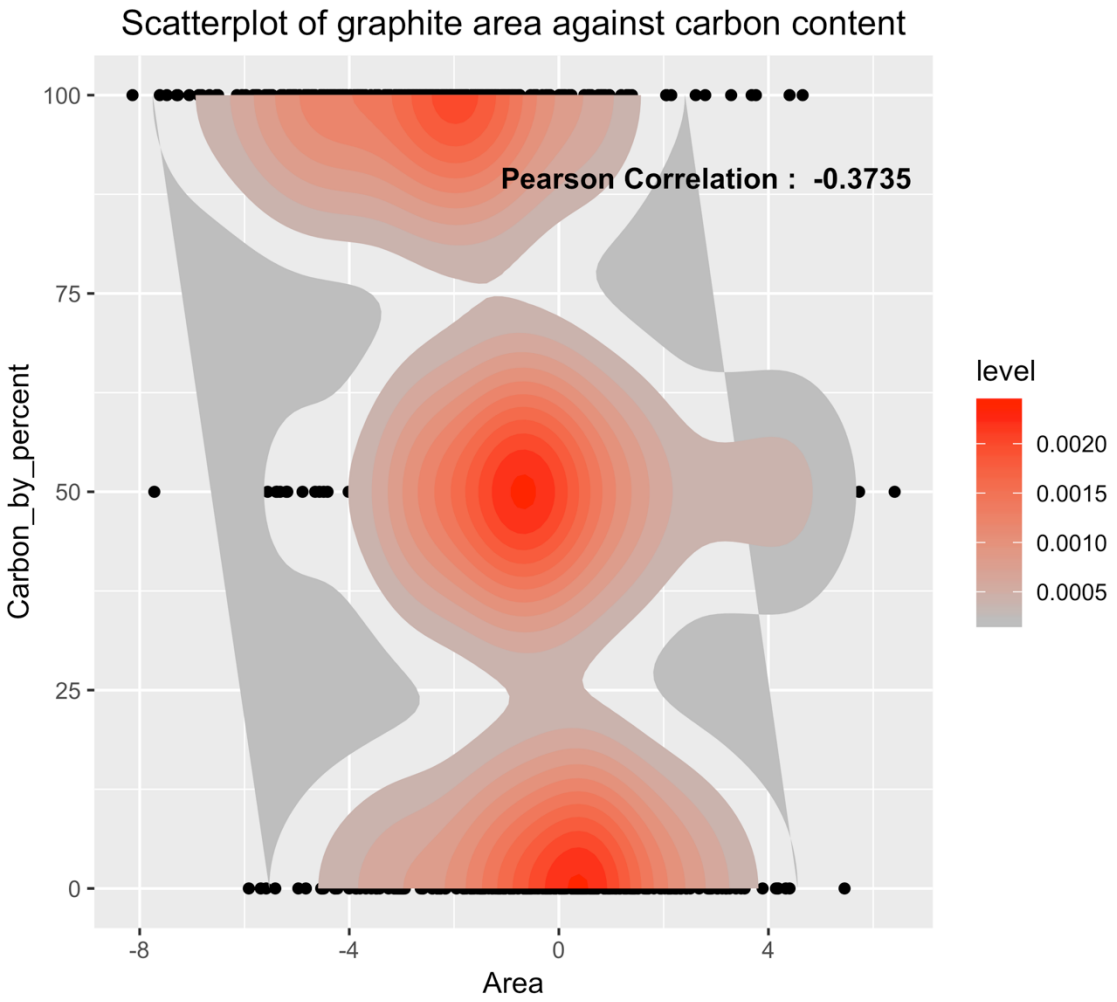

Figure 21. Scatterplot of graphite area against carbon content with correlation coefficient.

The color of red represented how the points dense together, and the Pearson correlation coefficient between graphite area and carbon content was -0.3753.

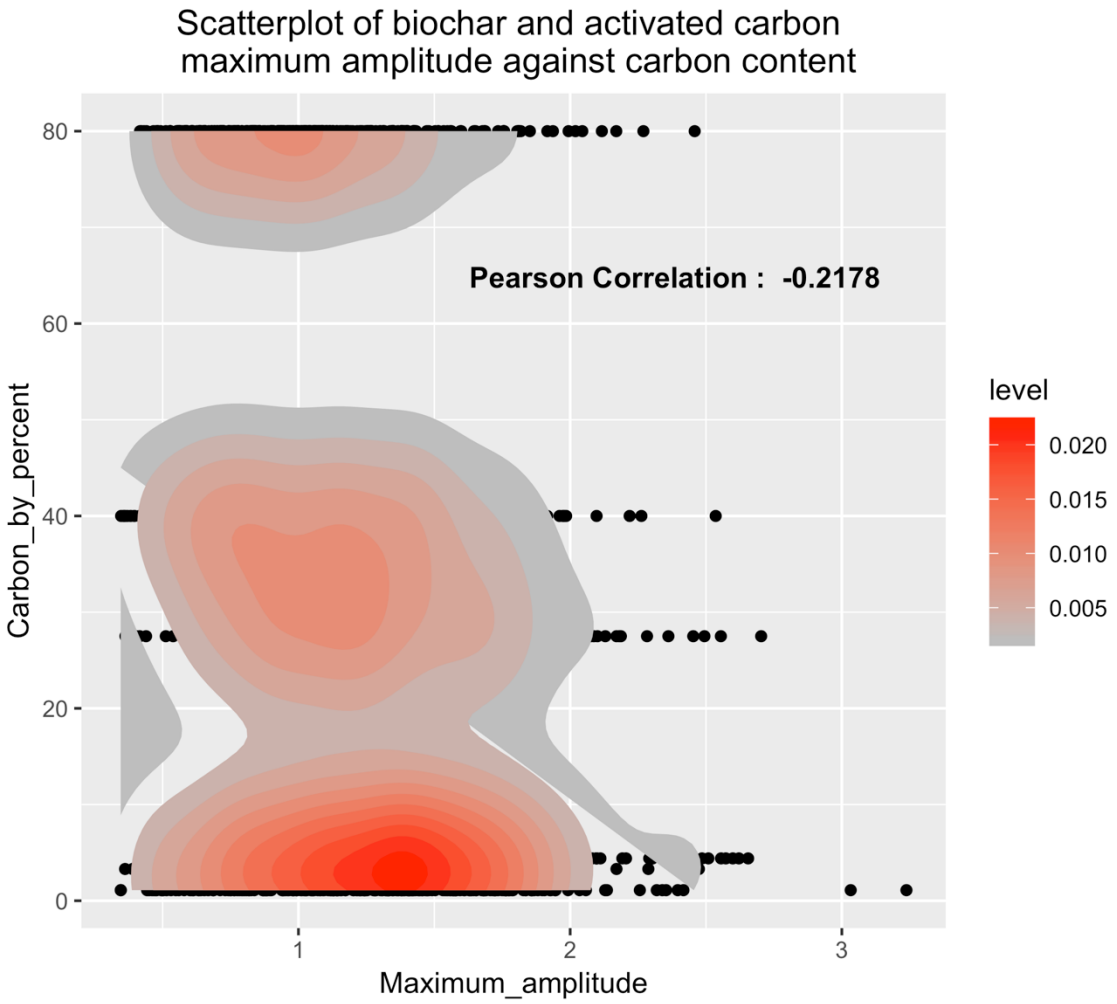

Figure 22. Scatterplot of biochar and activated carbon maximum amplitude against carbon content with correlation coefficient.

The color of red represented how the points dense together, and the Pearson correlation coefficient between biochar and activated carbon maximum amplitude and carbon content was -0.2178.

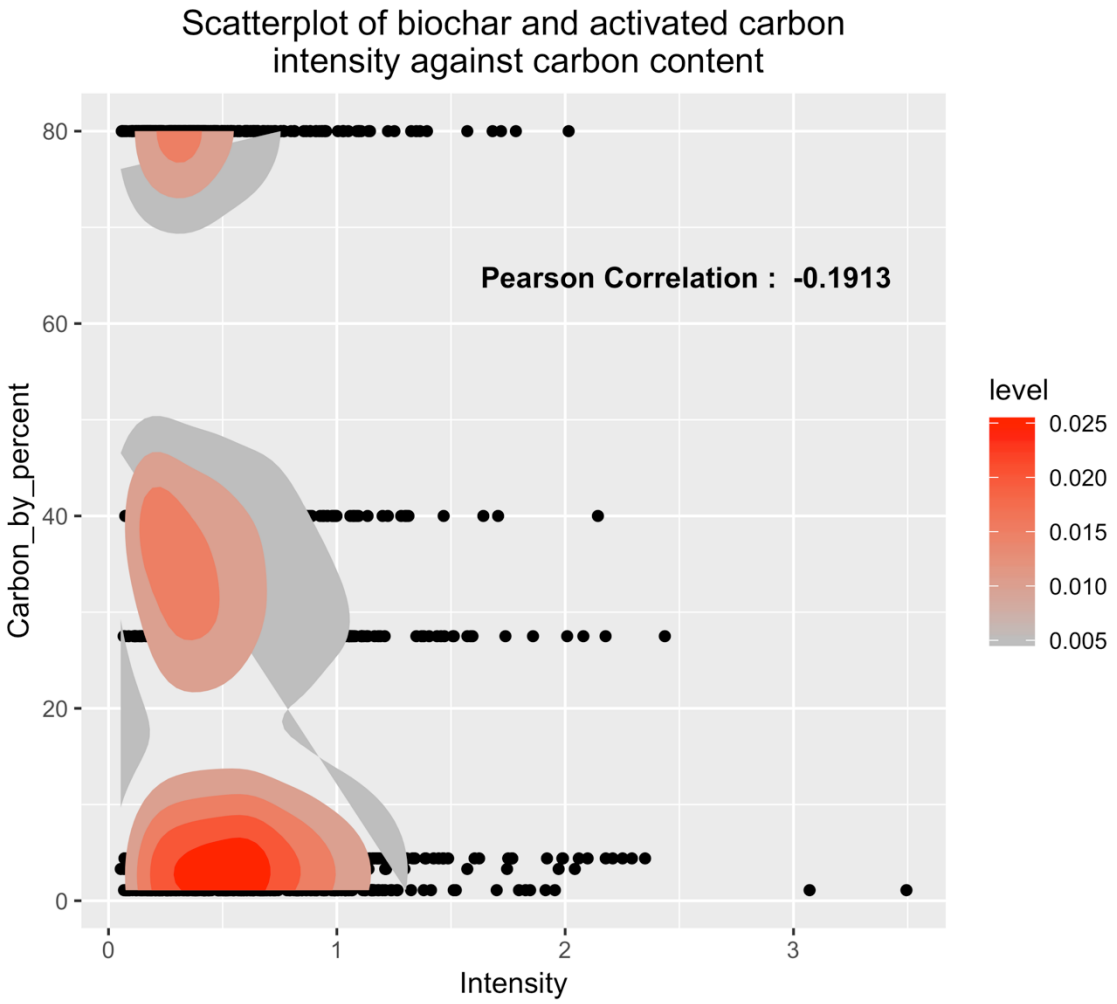

Figure 23. Scatterplot of biochar and activated carbon intensity against carbon content with correlation coefficient.

The color of red represented how the points dense together, and the Pearson correlation coefficient between biochar and activated carbon intensity and carbon content was -0.1913.

Figure 24. Scatterplot of biochar and activated carbon energy against carbon content with correlation coefficient.

The color of red represented how the points dense together, and the Pearson correlation coefficient between biochar and activated carbon energy and carbon content was -0.1937.

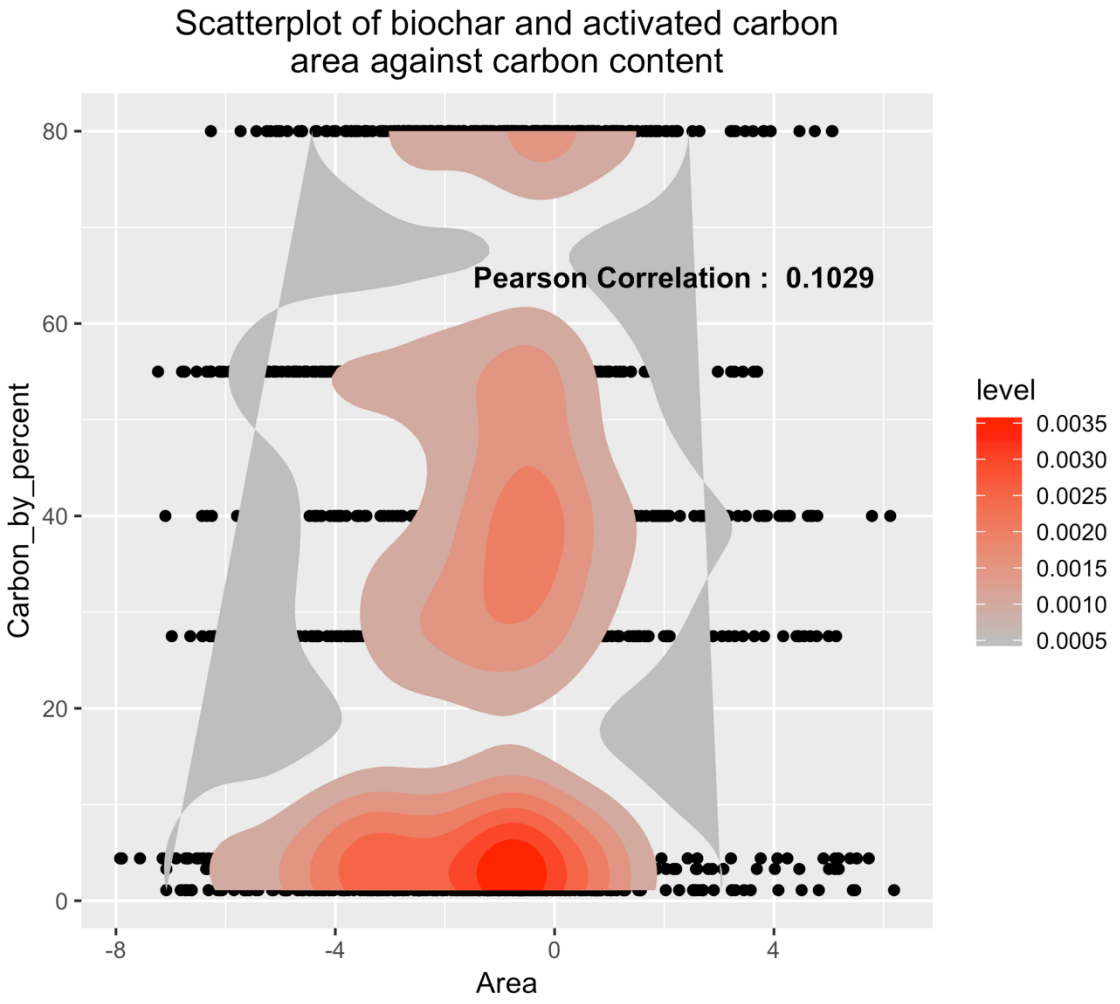

Figure 25. Scatterplot of biochar and activated carbon area against carbon content with correlation coefficient.

The color of red represented how the points dense together, and the Pearson correlation coefficient between biochar and activated carbon area and carbon content was 0.1029.